OXFORD
SOT | Society of Toxicology
academic.oup.com/toxsci

Toxicological Sciences, 2025, 1–21
https://doi.org/10.1093/toxsci/kfaf111
Advance Access Publication Date: July 30, 2025
Research article

A systems toxicology approach implicates post-transcriptional regulatory networks in reproductive defects from PFAS exposure

Abigail P. Bline[1], Hui Jiang[2], Max Levenson[1], Patrick Allard [1,2,3,*]

[1]Molecular Toxicology Interdepartmental Program, UCLA, Los Angeles, CA 90095, United States
[2]Institute for Society & Genetics, UCLA, Los Angeles, CA 90095, United States
[3]Molecular Biology Institute, UCLA, Los Angeles, CA 90095, United States

*Corresponding author: Institute for Society & Genetics, 611 Charles E Young Dr E, University of California, Los Angeles, Los Angeles, CA 90095, United States. Email: pallard@ucla.edu.

Abstract

Per- and polyfluoroalkyl substances (PFAS) are highly persistent in the environment and widespread in consumer products, environmental media, and biological samples. However, limited toxicology data exist for many of the over 15,000 chemicals belonging to the PFAS family. Data are particularly lacking for exposures during germ cell development, which can have consequences for later-life fecundity. Here, we leverage the tractability of the model organism *Caenorhabditis elegans* to compare a "legacy" PFAS, i.e. perfluorooctane sulfonic acid (PFOS), with a chlorinated ether analog, 6:2 chlorinated polyfluoroalkyl ether sulfonic acid (6:2 Cl-PFESA). We consistently observed negative effects of both PFOS and 6:2 Cl-PFESA on germ cell numbers along with increases in germline apoptosis and defective meiotic progression. These cellular observations corresponded with increases in embryonic lethality in offspring from developmentally exposed adults. Messenger RNA and small RNA sequencing revealed a clear signature of perturbation of the non-coding RNA-mediated germline regulatory network consistent with observed ex vivo disruption of P granules, liquid-like assemblages of RNA, and protein. Remarkably, we identified a strong gene–environment interaction between PFOS and 6:2 Cl-PFESA with another liquid-like structure, the synaptonemal complex (SC); *syp3(OK758)* hypomorphic mutants exhibited near-complete embryonic lethality with PFAS exposure. Thus, while performed at relatively high concentrations to ensure robust effect detection, our mechanistic findings provide a foundation for understanding the reproductive toxicity of PFAS across exposure scenarios. Altogether, our data show that the impacts of PFAS on germ cell development and function are associated with perturbation of liquid-like condensates, suggesting that PFAS physicochemical properties may contribute to their pleiotropic effects on biological systems.

Keywords: PFAS; toxicogenomics; biological condensates; reproduction; germ cells

Often referred to as "forever chemicals," per- and polyfluoroalkyl substances (PFAS) are a large class of anthropogenic molecules that exhibit high persistence in the environment. PFAS have been found in various consumer products, environmental media, and biological samples collected from humans and non-human animals across the globe (Kaboré et al. 2018; Nakayama et al. 2019). Within the human body, PFAS are unique among persistent organic pollutants in that they preferentially partition to proteins and membrane lipids of well-perfused organs rather than adipose tissue (Heuvel et al. 1991; Sanchez Garcia et al. 2018; Droge 2019). As a result, PFAS tend to distribute widely throughout the body, can accumulate in a variety of tissues, and have been associated with numerous health effects (Fenton et al. 2021).

Due to concerns about its health effects and persistence in the environment, US manufacturing of perfluorooctane sulfonic acid (PFOS), one of the most-studied PFAS, ceased in 2000 (US Environmental Protection Agency 2000). PFOS manufacturing and use was restricted in most countries by an international agreement in 2009 (United Nations Environment Program 2023). Even so, PFOS continues to be detected in serum in approximately 99% of US adults at a median concentration of approximately 5 ng/ml and remains a relevant human exposure (Calafat et al. 2019; Department of Health and Human Services, Centers for Disease Control and Prevention 2022). In recent years, 6:2 chlorinated polyfluoroalkyl ether sulfonic acid (6:2 Cl-PFESA), a chlorinated ether analog of PFOS, has been detected at comparably high frequencies and concentrations in human serum samples collected in China (He et al. 2022). A primary component of the formulation F-53B, 6:2 Cl-PFESA has been used since the 1970s as a PFOS alternative for mist suppression in the electroplating industry (He et al. 2022). Despite having been manufactured and used solely in China, 6:2 Cl-PFESA has been detected in surface water samples collected from the United States and Europe and in Arctic wildlife (Gebbink et al. 2016; Pan et al. 2018). Based on 2017 to 2018 National Health and Nutrition Examination Survey (NHANES) data, 6:2 Cl-PFESA was detected in approximately 12% of US adults at a median

serum concentration of 0.5 ng/ml (Centers for Disease Control and Prevention 2018). 6:2 Cl-PFESA is one of the most biopersistent PFAS currently in use, with a median total elimination time of over 15 years, making it a priority PFAS for further assessment (Shi et al. 2016). However, toxicity data on 6:2 Cl-PFESA are limited (Pelch et al. 2022).

Previous studies have found associations between PFOS exposure and increased risk of primary ovarian insufficiency as well as earlier age of natural menopause (Ding et al. 2020). These outcomes are dependent upon the establishment and maintenance of the ovarian reserve. Ovarian reserve establishment occurs prenatally in humans and other mammals (Vabre et al. 2017; Ge et al. 2019); primordial germ cell differentiation, proliferation, entry into meiotic prophase I, and physiologic oocyte death all occur prior to birth (De Felici et al. 2005). However, most studies on PFOS germ cell effects have examined exposures to postnatal ovaries or oocytes, which have ceased proliferation and already completed much of oogenesis (Domínguez et al. 2016; Chen et al. 2021; Wei et al. 2021; Feng et al. 2023; Clark et al. 2024). Although early developmental exposure to PFOS has shown negative effects on spermatogenesis and functional spermatids (Lai et al. 2017; Yin et al. 2021), data on the effects of early developmental PFOS or 6:2 Cl-PFESA exposure on oogenesis and oocyte function are lacking.

In the present study, we exposed *Caenorhabditis elegans* to PFOS or 6:2 Cl-PFESA from embryos to evaluate the effects of early developmental exposure on oogenesis and oocyte function. *C. elegans* serves as a particularly useful model for studying oogenesis because adult hermaphrodites continually generate oocytes in a linear arrangement along the gonad, from mitotic proliferation through all stages of meiosis, making cells in different phases of meiosis easy to visualize. They are also proven to be a particularly valuable model to assess the impact of various environmental agents on reproduction (Chen et al. 2016; Camacho et al. 2018; Chen et al. 2019; Wang et al. 2019; Truong et al. 2023; Ulaganathan et al. 2024). We performed standard reproductive assays, examined oogenic gonads microscopically, and analyzed gonad-specific RNA sequencing data to comprehensively evaluate PFOS and 6:2 Cl-PFESA exposures. We further assessed potential gene–environment interactions using two *C. elegans* mutant strains. We hypothesized that PFOS and 6:2 Cl-PFESA would similarly disrupt early germ cell development, leading to reproductive defects.

Materials and methods

Worm strains and culture

Unless otherwise stated, we used wild-type N2 Bristol strain *C. elegans* in experiments. Additional strains include the PGL-1::GFP reporter strain JH3269 (*pgl-1*[*ax3122*{*pgl-1*::*gfp*}] IV), the ZNFX-1::GFP/PGL-1::RFP reporter strain YY968 (*znfx-1*[*gg544*{*3xflag*::*gfp*::*znfx-1*}] II; *pgl-1*[*gg547* {*pgl-1*::*3xflag*::*tagRFP*}] IV), the *pgl-1(bn102)* loss-of-function mutant strain SS580, and the SYP-3::GFP reporter/partial rescue strain CA1218 (*syp-3*[*ok758*] I; ieSi11 [*syp-3p*::*EmeraldGFP*::*syp-3*::*syp-3* 3'UTR + Cbr-*unc-119*(+)] II; *unc-119* [*ed3*] III). Other than the N2 worms, we obtained worm strains from the University of Minnesota Caenorhabditis Genetics Center (CGC). We maintained worms at 20 °C on nematode growth medium (NGM) with OP50 *Escherichia coli* lawns for both culturing and experimental procedures.

Test compounds and solution preparation

We purchased PFOS (CAS number 1763-23-1, >99.5%) from Synquest Laboratories. 6:2 Cl-PFESA potassium salt (CAS number 73606-19-6) was purchased from BOC Sciences as technical grade to reflect real-world exposure. For each experimental repeat, we prepared solutions freshly from solid powders dissolved directly in double-deionized water that was filtered through a 0.22 μm membrane filter. For positive controls in the embryonic lethality and/or ex vivo P granule assays, we used nocodazole (CAS number 31430-18-9) and 1,6-hexanediol (CAS number 629-11-8). Stock solutions of nocodazole were prepared in DMSO, whereas 1,6-hexanediol solutions were prepared in double-deionized water.

In vivo worm exposures

We exposed *C. elegans* to PFOS or 6:2 Cl-PFESA on solid NGM treated with liquid solutions as previously described (Nass and Hamza 2007; Xiong et al. 2017). We applied PFAS solutions or filtered double-deionized water (negative control) to the surface of NGM-filled plates with OP50 *E. coli* lawns at a ratio of 1:45 on a volume-for-volume basis (e.g. 0.4 ml of PFAS solution or water applied to 18 ml of solid NGM). Based on previous findings on measured internal PFOS concentrations in *C. elegans* exposed using similar methods, we estimated that application of a 1,100 μM PFOS solution to solid NGM should lead to an internal dose of approximately 4 parts per billion, which is within an order of magnitude of PFOS and 6:2 Cl-PFESA serum concentrations measured in the general US population (Centers for Disease Control and Prevention 2018; Stylianou et al. 2019; Bil et al. 2022). Therefore, we used 1,100 μM plus 4 additional liquid solution concentrations (900, 450, 225, and 112.5 μM) to treat the solid NGM in our initial embryonic lethality range-finding experiment. Subsequent in vivo assays used the no observable effect concentration (225 μM liquid solution), the lowest observable effect concentration (450 μM liquid solution), and double the LOEC (900 μM liquid solution) from the range-finding experiment.

We exposed *C. elegans* to the PFAS- or water-treated NGM starting as embryos. We used a modified timed egg-laying protocol to obtain synchronized *C. elegans* populations for experiments (Lionaki and Tavernarakis 2013; Lancaster et al. 2022). Briefly, we picked L4 stage larval worms from standard NGM culture plates onto new plates and allowed the larvae to grow to adulthood (approximately 24 h). We transferred 10 of the adult *C. elegans* to PFAS- or water-treated NGM plates and allowed them to lay embryos for 2 to 3 h, resulting in approximately 100 to 150 embryos per NGM plate. After this time, we removed the adult *C. elegans* and left the remaining embryos to develop on the treated NGM for use in the in vivo assays described below.

Embryonic lethality

We let embryos (P0 generation) develop on treated NGM plates to day 1 of adulthood. We randomly selected 4 to 10 P0 adults from each treatment and transferred them to new NGM plates with the same treatment. We left the P0 adult worms on the new NGM plates to lay embryos (F1 generation) for approximately 4 to 6 h. After this time, we removed the P0 adults from the plates and counted the number of F1 embryos under a dissecting microscope. We allowed F1 embryos to develop until the late L4 or early adult stage, at which point we counted the surviving F1 worms. We calculated embryonic lethality as the percentage of F1 embryos laid on an NGM plate that failed to hatch or produce viable late larvae/early adults.

Gonad dissection, immunofluorescence, and imaging

Due to differences in developmental timing between exposure groups, we collected all worms for gonad imaging at 96 h post-embryo, by which time worms in all exposure groups had reached the adult stage. We performed fixation and staining of the worms as previously described (Gervaise and Arur 2016; Das et al. 2020). We use the following primary and secondary antibodies and concentrations: 1:500 mouse anti-mitogen-activated protein kinase (MAPK)-YT (Sigma-Aldrich, M8159), which is reactive against *C. elegans* diphosphorylated MPK-1 (Achache et al. 2019; Das et al. 2020); 1:7.5 mouse anti-PGL-1 (Developmental Studies Hybridoma Bank, OIC1D4-s, 39 μg/ml); 1:500 Cy3 goat anti-mouse (ABclonal, Inc., AS008) (for dpMPK-1); 1:500 Alexa Fluor 594 donkey anti-mouse (Jackson ImmunoResearch Inc., 715-585-150) (for PGL-1).

We imaged gonads using a Nikon H600L epifluorescence microscope at 100× magnification. Stages of meiosis were identified based on chromosome morphology. We conducted image processing and measurements with the Fiji software. Nuclei in each developmental stage were quantified using the cell count feature. We calculated average anti-dpMPK-1 fluorescence intensity using manually defined regions in the mitotic zone, the late pachytene zone, and the diplotene/gonad bend region of each gonad. We calculated the dpMPK-1 fluorescence intensity ratios between different regions within the same gonad. Intensity ratios were normalized by the mean intensity ratio across treatment groups within each experimental repeat. We calculated average PGL-1 granule size by measuring the diameter of one representative granule from 5 separate nuclei in the late pachytene region of each gonad.

Brood size and lifespan

We let embryos (P0 generation) develop on treated NGM plates for approximately 48 h and transferred 5 worms from each treatment onto individual NGM plates of the same treatment. It should be noted that the PFAS-exposed worms developed more slowly than the water control worms. We transferred worms to new NGM plates of the same treatment every 12 h for the duration of their reproductive lifespans (approximately 5 days). Approximately 72 to 96 h after we transferred a P0 adult from an NGM plate, we counted the number of late larval/early adult F1 worms on the same plate. We calculated the viable brood size as the total number of surviving late larval/early adult F1 worms produced per P0 worm. Assay validity was based on control worms producing a mean brood size of at least 200 live offspring. One experimental repeat for 6:2 Cl-PFESA exposure did not meet this validity criteria and was excluded from analysis.

Germ cell apoptosis

Approximately 24 h post-L4, we removed 50 worms from their treated NGM plates and incubated them for 1 h in a 25 μg/ml solution of acridine orange diluted in M9 minimal salts solution supplemented with OP50 *E. coli*. Worms grown on NGM treated with 450 μM and 900 μM PFAS were incubated in acridine orange a day later than those grown on water-treated NGM and NGM treated with 225 μM PFAS due to the delayed development of the former groups. Immediately following acridine orange incubation, we imaged live worms with a Nikon H600L epifluorescence microscope at 40× magnification. We scored apoptotic germ cell nuclei as FITC-positive foci in the late pachytene region of a single gonad arm. To account for differences in the number of germ cells in each gonad between treatments, we calculated the apoptotic index as the number of apoptotic nuclei divided by the mean number of pachytene nuclei for the treatment group. The apoptotic index was normalized to the mean apoptotic index across treatment groups within each experimental repeat.

Gonad collection and RNA extraction

We let synchronized N2 embryos develop on treated NGM plates for 96 h. We selected only negative control worms and worms exposed to 450 μM 6:2 Cl-PFESA for gonad RNA analysis since mRNA levels have previously been measured in whole worms exposed to PFOS (Chen et al. 2018; Stylianou et al. 2019), but not in worms exposed to 6:2 Cl-PFESA, and since 450 μM was the LOEC for most of the endpoints examined in this study. We collected 12 adult worms from a given treatment and pooled their severed gonads into a 1.5 ml low-binding microcentrifuge tube set in a freezing block on dry ice to flash-freeze. For each batch of 12 worms, the time from gonad dissection to flash-freezing did not exceed 10 min. We repeated this process 12 times for each treatment (NGM treated with water or 450 μM 6:2 Cl-PFESA) such that we collected gonads from approximately 140 worms per treatment for each of the 3 experimental repeats.

We extracted RNA from the pooled gonads using the QIAGEN miRNeasy Micro Kit (217084). We evaluated the quantity and purity of RNA using a NanoDrop spectrophotometer. We immediately split the extracted RNA samples, with half of the sample volume frozen at −80 °C for mRNA sequencing. We subjected the other half to treatment with RNA 5′ polyphosphatase (Epicentre, RP8092H) to remove tri- and diphosphate modifications from small RNAs for sRNA sequencing. Briefly, the aqueous RNA samples were combined with RNA 5′ polyphosphatase 10× reaction buffer, RNA 5′ polyphosphatase, and additional RNase-free water and incubated at 37 °C for 30 min. After incubation, we re-purified the RNA using the QIAGEN miRNeasy Micro Kit, omitting the QIAzol lysis reagent step. We then froze the RNA 5′ polyphosphatase-treated RNA at −80 °C for sRNA sequencing.

P granule structure with in vivo exposure

We let PGL-1::RFP reporter strain YY968 embryos develop on treated NGM plates for approximately 96 h. We picked ∼30 adult worms into a 14 μl drop of M9 minimal salts solution placed on a microscope slide, to which 1 μl of 10 mM levamisole hydrochloride was added to immobilize the worms. We imaged the pachytene regions of immobilized worms using the Texas Red filter of a Nikon H600L epifluorescence microscope at 100× magnification.

Synthetic sterility in a pgl-1 loss-of-function mutant

We let *pgl-1(bn102)* loss-of-function strain SS580 embryos develop on treated NGM for approximately 96 h. We scored adult worms exhibiting one or more embryos in their uteri as fertile. Worms lacking embryos and exhibiting a degenerated and/or malformed gonad were scored as sterile. We did not count worms that lacked embryos but appeared to be young adult or in the L4 larval stage based upon gonad morphology since the lack of embryos could have been due to developmental delay rather than sterility.

Ex vivo gonad exposures

We picked unexposed day 1 adult worms into an 8 μl drop of M9 minimal salts solution on a microscope slide. We extruded the gonads from the worms and added 8 μl of a PFOS or 6:2 Cl-PFESA solution prepared in filtered double-deionized water or filtered double-deionized water alone (negative control). We mixed this solution with the drop of M9 using a 10 μl pipette tip. Final ex vivo PFAS exposure concentrations were 10 and 450 μM, which

represented the estimated NGM exposure concentration (10 μM) and the initial solution concentration (450 μM) applied to the NGM that was the LOEC in vivo experiments. We then covered the dissected gonads in treatment solutions with cover slips for imaging.

P granule structure ex vivo

We used the PGL-1::GFP reporter strain JH3269 to visualize P granules ex vivo. We used a solution of 5% 1,6-hexanediol in double-deionized water as a positive control for P granule structure disruption (Updike et al. 2011). We imaged the dissected gonads using the FITC filter of a Nikon H600L epifluorescence microscope at 40× magnification. Specifically, we imaged the pachytene region of a different worm every 4 min for 16 min on each slide to monitor time-dependent effects of *ex vivo* PFAS exposure on P granule structure.

SC structure ex vivo

We used the SYP-3::GFP reporter/*syp-3(ok758)* partial rescue strain CA1218 to visualize the SC ex vivo. A solution of 5% 1,6-hexanediol in double-deionized water was used as a positive control for SC structure disruption (Rog et al. 2017). We imaged the dissected gonads with the FITC filter of a Nikon H600L epifluorescence microscope at 100× magnification.

RNA sequencing and bioinformatics

Frozen RNA samples were provided to the UCLA Technology Center for Genomics & Bioinformatics (TCGB) for cDNA library construction and sequencing. The library for mRNA sequencing was constructed from the sample volumes not treated with RNA 5′ polyphosphatase using the KAPA mRNA HyperPrep Kit for Illumina platforms (Kapa Biosystems, KR1352-v5.17). The library for sRNA sequencing was constructed from the sample portions treated with RNA 5′ polyphosphatase using the QIAseq microRNA (miRNA) Library Kit (QIAGEN, 331502). After checking RNA integrity using an Agilent TapeStation system, single-read RNA sequencing was performed using an Illumina HiSeq 3000 system. TCGB provided demultiplexed FASTQ files with the Illumina adapters removed.

mRNA data analysis

We uploaded the FASTQ files to Galaxy and checked read quality using FastQC. Transcripts were quasi-mapped to the WormBase WS287 mRNA transcripts FASTA file (Index of/releases/WS287/species/c_elegans/PRJNA13758) and transcript counts were quantified using the Salmon quant tool (Galaxy Version 1.10.1+galaxy0) (Patro et al. 2017; Srivastava et al. 2019). We used the WormBase WS287 genomic FASTA file as the reference genome. We set K-mer length to 25 with a perfect hash required. We set sequence-specific strand correction and GC fragment correction to "yes" since FastQC results indicated that GC sequences were overrepresented in the mRNA data. We set the mean fragment size to 65 since this was the size identified by FastQC analysis.

We performed differential expression analysis between the control and 6:2 Cl-PFESA mRNA samples in Galaxy using the DESeq2 tool (DESeq2 version 1.40.2, Galaxy Version 2.11.40.8+galaxy0) on the Salmon quant transcript count data (Love et al. 2014). We performed gene set enrichment analysis using PANGEA against the direct gene ontology (GO) data set and using WormExp v 2.0 against *C. elegans*-specific experimental data sets (Yang et al. 2016; Hu et al. 2023). For both PANGEA and WormExp analyses, we analyzed the most significantly upregulated and downregulated genes (based on DESeq2 Benjamini-Hochberg adjusted *P*-value <0.05) as separate gene sets. We used all genes detected in the gonad mRNA samples ($n = 15{,}733$) as the background gene set for both analyses. We refined WormExp results for relevance based on the following: (i) the Bonferroni-adjusted *P*-value for enrichment was <0.05, (ii) at least 15 significantly upregulated or downregulated genes overlapped with the gene set, and (iii) the gene set originated from adult hermaphrodite worm gonads or whole animals.

sRNA data analysis

We uploaded FASTQ files to sRNAbench, part of the sRNAtoolbox (Aparicio-Puerta et al. 2022). sRNAbench preprocesses the FASTQ file, aligns the reads to the genome using Bowtie, and quantifies reads. We ran sRNAbench in genome mapping mode using the MirGeneDB2.1 database, WBcel235 *C. elegans* genome assembly, Qiagen with UMIs library protocol, minimum mean Phred score per transcript set to 20, and the remaining parameters set to the default values. We extracted 21U-RNA (i.e. Piwi-interacting RNA [piRNA]), 22G-RNA, 26G-RNA, and miRNA reads from the sRNAbench annotated reads file generated for each sample using a custom R script (with dplyr, purr, and stringr packages).

To obtain 21U-RNAs/piRNAs, we first filtered the reads by the RNA Central sense classification. We further filtered by reads annotated as either piRNA or other RNA (excluding those additionally annotated as ncRNA, snRNA, or snoRNA) with sequence length equal to or less than 21 nucleotides and the first nucleotide equal to T. We aggregated read counts by the feature to which they were annotated. To obtain 22G-RNAs and 26G-RNAs, we first filtered the reads by the cDNA antisense, tRNA antisense, ncRNA antisense, and RNA Central antisense classifications. For 22G-RNAs, we then filtered the reads by sequence length equal to 20 to 24 nucleotides and the first nucleotide equal to G (Seroussi et al. 2023). For 26G-RNAs, we filtered the reads by sequence length equal to 25 to 27 nucleotides and first nucleotide equal to G (Seroussi et al. 2023). We aggregated 22G-RNA and 26G-RNA read counts by the target feature to which they were antisense within each sample. To obtain miRNAs, we filtered the reads by the mature sense classification. We aggregated read counts by the feature to which they were annotated.

For each sRNA type, we removed features that did not have at least 10 reads in at least 2 samples. We calculated the number of reads for each sRNA type as reads per million (RPM) genome-mapping reads, excluding sense protein-coding, pseudogene, tRNA, rRNA, ncRNA, lncRNA, and snoRNA reads within each sample. These sense-mapping reads likely represent degradation products and not sRNAs (Seroussi et al. 2023). For comparisons of each sRNA type between treatments, we normalized sRNA RPMs to the mean across treatments within each experimental repeat. We performed DESeq2 analysis for each sRNA type in Galaxy using reads aggregated by feature. We further tested targets of differentially expressed 22G-RNAs for enrichment or depletion relative to Argonaute immunoprecipitation (IP) data reported by Seroussi et al. (2023). Of the 19 Argonautes with 22G-RNA IP data, ALG-1, ALG-2, and ALG-5 were excluded from comparison, as they primarily bind miRNAs and have fewer than 100 non-miRNA targets. We determined significant overlap between 22G-RNA targets upregulated or downregulated by 6:2 Cl-PFESA treatment and those that IP with a given Argonaute using the hypergeometric distribution with the total number of 22G-RNA targets detected in the gonad samples prior to trimming (14,933) as the population size. We adjusted *P*-values for multiple testing using the Bonferroni correction.

Statistical analysis

For between-group comparisons of normally distributed data, we used Welch's ANOVA with Dunnett's T3 post-hoc test for statistical analyses to account for unequal variances and small degree of freedom. We used linear regression or Poisson regression with offset for treatment group size to assess trends. We used Welch's *t*-test for comparisons with only 2 groups. We performed statistical analyses and figures generation using R statistical software version 4.2.0 (Ripley 2001) and GraphPad Prism 10.

Results

PFOS and 6:2 Cl-PFESA increase embryonic lethality in wild-type *C. elegans*

To identify the relevant concentrations of PFOS and 6:2 Cl-PFESA in our subsequent assays, we first performed range-finding experiments using embryonic lethality as the endpoint. Embryonic lethality can serve as a readout for various errors that occur during meiotic prophase I and ultimately lead to aneuploidy (Lui and Colaiácovo 2013). The lowest observed effect concentration for PFOS was 900 μM applied to solid NGM (Fig. 1A), whereas it was 450 μM for 6:2 Cl-PFESA (Fig. 1B). At the highest concentration of 1,100 μM applied to solid NGM, the maximal effect was a mean embryonic lethality incidence of 18% (95% CI: 4–31; $P = 0.01$) for PFOS and 23% (95% CI: 13–34; $P = 0.0004$) for 6:2 Cl-PFESA. These effects were comparable to those from exposure to solid NGM treated with 900 μM of the positive control nocodazole (Fig. 1A and B). In liquid exposure scenarios, 100 μM nocodazole leads to an approximate embryonic lethality incidence of 65% (Allard et al. 2013), similar to the effect we observed with 4.5 mM of nocodazole applied to solid NGM (Fig. 1A). Although the solution concentrations used are substantially higher than typical human serum concentrations, these findings support our assumption that the final concentrations on the solid NGM were approximately 45 times lower than the applied solution concentrations (corresponding to the 1:45 volume-for-volume dilution factor).

We also included 1,6-hexanediol as a comparator in the embryonic lethality assay. 1,6-hexanediol is an aliphatic alcohol that has been shown to increase DNA double-strand breaks, which can lead to embryonic lethality when unrepaired in germ cells (Lemmens and Tijsterman 2011; Jones and Forsburg 2023; Gombás and Villányi 2024). Importantly, 1,6-hexanediol inhibits liquid–liquid phase separation (LLPS) in various biological contexts, an effect that may be shared by PFOS and 6:2 Cl-PFESA due to their surfactant properties (Buck et al. 2011; Sanchez-Burgos et al. 2021). Worms exposed to NGM treated with a saturated solution of 1 g/ml 1,6-hexanediol exhibited a mean embryonic lethality incidence of 14% (95% CI: 7–20; $P = 0.0005$) (Fig. 1B).

PFOS and 6:2 Cl-PFESA cause delays in reproductive development and negatively impact fecundity

Because we observed increases in embryonic lethality, we examined additional effects of PFOS and 6:2 Cl-PFESA on reproduction over the life course. We specifically assessed developmental timing and production of live offspring since these outcomes have been shown to be altered in response to various well-known reproductive toxicants (Allard et al. 2013; Parodi et al. 2015; Chen et al. 2016). The mean time to first brood was approximately 2.9 days in control worms. In worms exposed to solid NGM treated with 900 μM PFOS, time to first brood was delayed by an average of 9 h (Fig. 2A). This delay was approximately 21 h in worms exposed to solid NGM treated with 900 μM 6:2 Cl-PFESA (Fig. 2B).

Across experimental repeats, control worms exhibited a mean viable brood size of 230. Based on linear regression modeling, PFOS exposure caused a decreasing trend in total viable brood size ($F(1,10)=9.22$, adjusted $R^2=0.43$; $P = 0.01$) (Fig. 2C). 6:2 Cl-PFESA exposure led to a similar decreasing trend in total viable brood size ($F(1,10)=6.43$, adjusted $R^2=0.33$; $P = 0.03$) (Fig. 2D). Group-based comparisons did not reach statistical significance. However, exposure to solid NGM treated with 900 μM caused a significant decrease in peak reproductive output per 12-h period (Fig. S1).

PFOS and 6:2 Cl-PFESA decrease meiotic germ cell abundance, inhibit differentiation, and increase apoptosis

To further evaluate the impact of PFOS and 6:2 Cl-PFESA on germ cells, we examined gonads from wild-type worms exposed in vivo from embryos through adulthood. Gonads dissected from adult hermaphrodites exposed to PFOS and 6:2 Cl-PFESA were visibly smaller than those from control worms, particularly in the highest exposure groups (Fig. 3A to G). Based upon imaging of DAPI-stained gonad nuclei, both PFOS and 6:2 Cl-PFESA exposures caused decreases in oogenic nuclei counts. Proliferating germ cell counts in the mitotic zone were reduced by approximately 35% (95% CI: 3–69; $P = 0.04$) and 41% (95% CI: 6–78; $P = 0.03$) with the highest PFOS (Fig. 3H) and 6:2 Cl-PFESA (Fig. 3J) exposures, respectively. Effects on meiotic germ cell nuclei were even greater, with mean counts reduced by approximately 60% for both the highest PFOS (95% CI: 39–79; $P = 0.001$) (Fig. 3I) and 6:2 Cl-PFESA (95% CI: 26–94; $P = 0.007$) exposures (Fig. 3K).

Because meiotic germ cell nuclei counts were significantly reduced by exposure to these two PFAS, we then tested whether meiosis proceeded correctly. Under normal conditions, oogenic germ cell nuclei transition from pachytene to diplotene just distally to the gonadal arm bend (Fig. 4A). Failure to properly progress through meiosis can manifest as the presence of pachytene nuclei beyond the bend and into the proximal gonad, a phenotype referred to as pachytene exit (Pex) defect (Killian and Hubbard 2005) (Fig. 4B and C). We observed the Pex defect in a single control worm. Based on Poisson regression with offset for treatment group size, PFOS exposure caused an increase in Pex incidence with increasing concentration (McFadden pseudo-$R^2 = 0.56$, $P < 0.001$) (Fig. 4D). Increasing Pex incidence was also observed with increasing 6:2 Cl-PFESA concentrations (McFadden pseudo-$R^2 = 0.37$, $P = 0.004$) (Fig. 4E).

Next, we examined the induction of apoptosis in mid to late pachytene, where it is physiologically triggered in response to meiotic checkpoint activation (Leacock and Reinke 2006). Because PFAS treatments significantly reduced the total number of pachytene nuclei available to undergo apoptosis, we calculated the apoptotic index by dividing the number of apoptotic nuclei by the mean number of pachytene germ cell nuclei for the given treatment. The apoptotic index was significantly increased in worms exposed to NGM treated with both 450 and 900 μM PFOS (Fig. 4F) or 6:2 Cl-PFESA (Fig. 4G).

The results of these reproductive assays indicate that PFOS and 6:2 Cl-PFESA exposures delay reproductive system development and decrease the number of oogenic germ cells produced. The germ cells that are produced in PFAS-exposed worms exhibit defects that lead to meiotic progression delays and/or apoptosis. Although the impacts of these defects on fecundity were subtle,

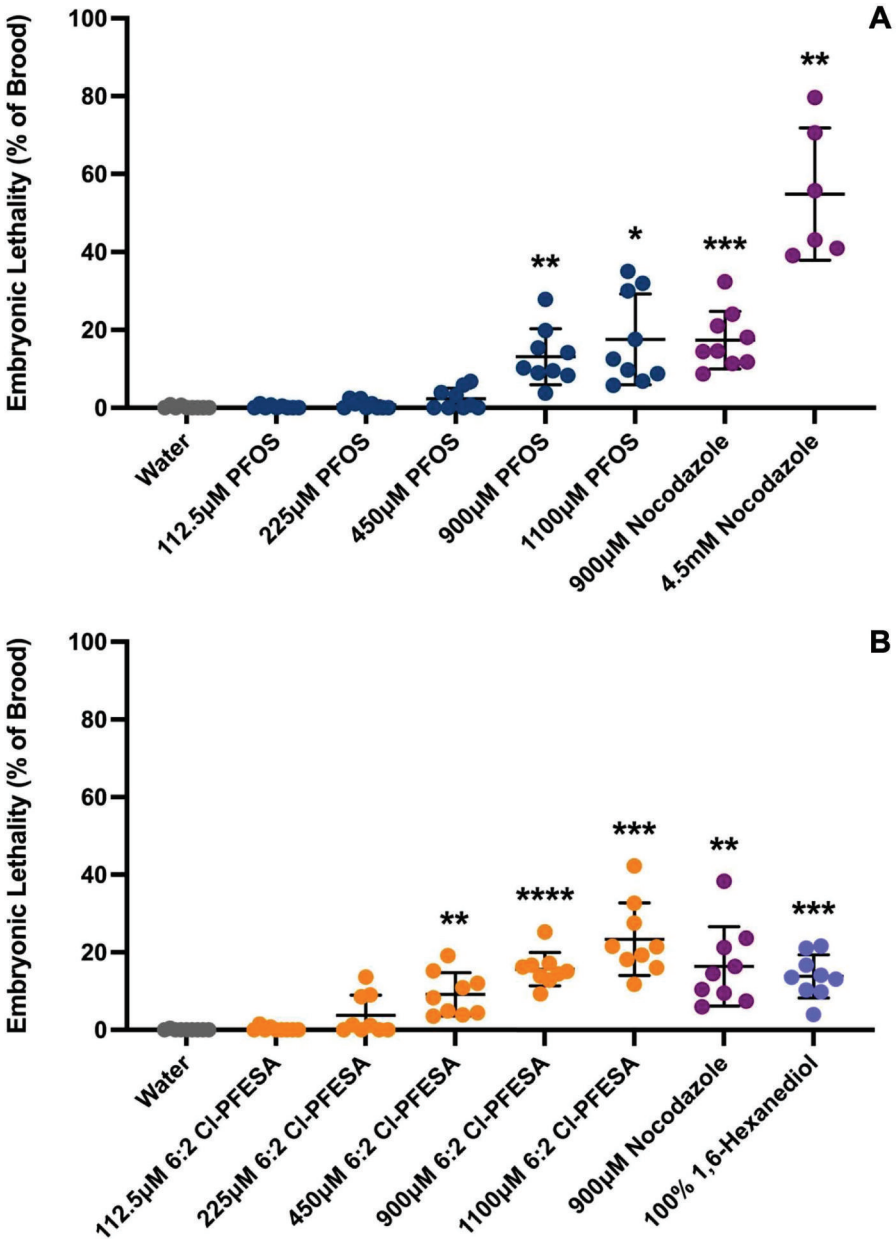

Fig. 1. Embryonic lethality is increased with PFOS or 6:2 Cl-PFESA exposure. *Caenorhabditis elegans* exposed to NGM treated with (A) 900 or 1,100 μM PFOS or (B) 450, 900, or 1,100 μM 6:2 Cl-PFESA exhibited increased rates of embryonic lethality. The rates of embryonic lethality caused by PFOS or 6:2 Cl-PFESA exposure were similar to those of exposure to NGM treated with (A, B) the positive control chemical nocodazole at 900 μM and (B) the positive control 100% 1,6-hexanediol. Exposure to NGM treated with 4.5 mM nocodazole caused approximately 60% embryonic lethality on average, a rate similar to liquid exposures in 100 μM nocodazole in our lab. Concentrations are reported as the concentrations of treatment solutions applied to solid NGM at a ratio of 1:45 volume to volume. Each point represents the % embryonic lethality from 5 to 10 individual *C. elegans* exposed on a single NGM-containing plate. $n = 9$ independent NGM plates per treatment, except n = 6 independent NGM plates for 4.5 mM nocodazole. Error bars represent mean and standard deviation. $^{*}P < 0.05$, $^{**}P < 0.01$, $^{***}P < 0.001$, $^{****}P < 0.0001$ (one-way Welch's ANOVA with Dunnett's T3 post hoc).

they suggest that germ cell signaling programs and homeostasis are disrupted by PFOS and 6:2 Cl-PFESA exposures.

Inappropriate MAPK activation in the gonad suggests multiple pathways are involved in germ cell dysfunction

MAPK signaling pathways are known to play important roles in germ cell development and function in *C. elegans*, as well as in other organisms (Lee et al. 2007a, 2007b; Das and Arur 2017). In *C. elegans*, activity of the human MAPK1/ERK2 ortholog MPK-1 regulates a wide range of processes in germ cells, including pachytene progression, apoptosis, and oocyte meiotic maturation (Church et al. 1995; Lee et al. 2007a, 2007b; Nadarajan et al. 2016). MPK-1 is typically activated through diphosphorylation via upstream signaling from DAF-2 (an insulin-like receptor) in the mid- to late-pachytene region and via major sperm protein signaling in proximal oocytes (Miller et al. 2001; Lopez et al. 2013). In wild type worms, dpMPK-1 levels are highest in mid to late pachytene and proximal oocytes, with lower levels in the gonad bend located between these 2 regions (Lee et al. 2007b). dpMPK-1 is not typically observed in the mitotic or early pachytene regions, where it is inhibited by a combination of RAS GTPase-activating protein GAP-3 and Pumilio protein PUF-8 (Vaid et al. 2013). *mpk-1* loss-of-function mutants, as well as loss-of-function

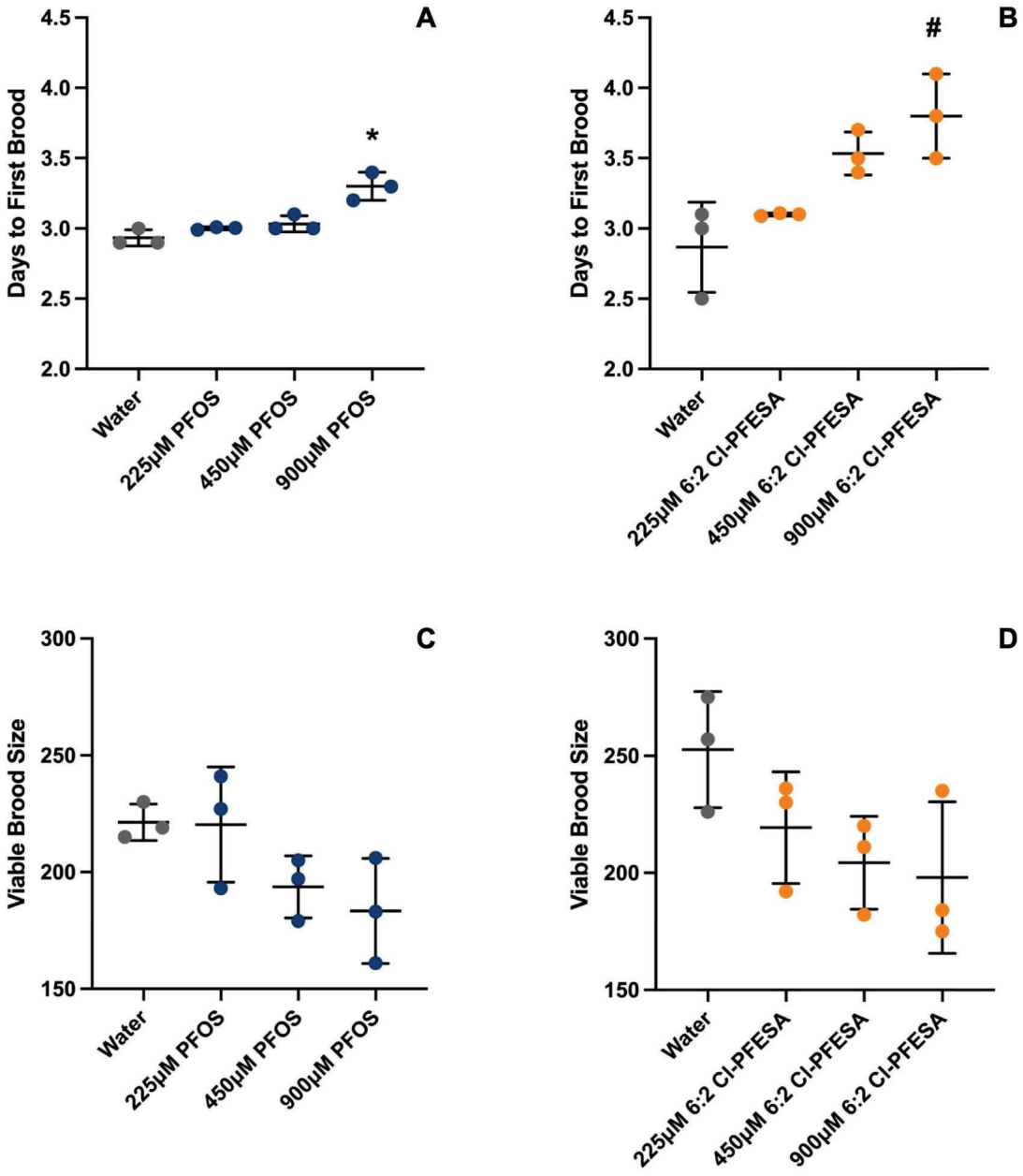

Fig. 2. Exposure to PFOS and 6:2 Cl-PFESA cause functional reproductive defects. Exposure to NGM treated with 900 μM of (A) PFOS or (B) 6:2 Cl-PFESA increased the time to first brood. Increasing concentrations of (C) PFOS or (D) 6:2 Cl-PFESA also caused significant decreasing trends in viable brood size based on linear regression modeling, though between-group comparisons were not significant. Concentrations are reported as the concentrations of solutions applied to solid NGM at a ratio of 1:45 volume to volume. Each point represents the mean of 4 to 5 individual *C. elegans* exposed on a single NGM-containing plate. $n = 3$ independent NGM plates per treatment. Error bars represent mean and standard deviation. $^{\#}P < 0.10$, $^{*}P < 0.05$ (one-way Welch's ANOVA with Dunnett's T3 post hoc).

mutants in upstream MAPK signaling genes, exhibit small gonads, Pex defects, and elevated embryonic lethality (Leacock and Reinke 2006; Achache et al. 2019). Therefore, we hypothesized that PFOS and 6:2 Cl-PFESA exposure may lead to these observed effects via impaired MPK-1 activation.

Contrary to our hypothesis, immunofluorescence imaging revealed that PFAS-exposed worms exhibited high levels of dpMPK-1 in the mid- to late-pachytene region and proximal oocytes, as was expected and observed in control animals (Fig. 5A to C). Unexpectedly, worms exposed to NGM treated with 900 μM PFOS exhibited a significant increase in dpMPK-1 intensity in the mitotic region relative to pachytene (Fig. 5D). We did not observe this effect in worms exposed to 6:2 Cl-PFESA (Fig. 5E). In worms exposed to NGM treated with 900 μM PFOS or 6:2 Cl-PFESA, we observed a near significant ($P < 0.10$) increase in dpMPK-1 intensity in the gonad bend region relative to pachytene (Fig. 5F and G). Linear regression modeling indicated there was an increasing trend in relative bend: pachytene dpMPK-1 intensity with both increasing PFOS ($F(1, 10) = 18.13$, adjusted $R^2 = 0.61$, $P = 0.002$) and 6:2 Cl-PFESA ($F(1, 10) = 11.29$, adjusted $R^2 = 0.48$, $P = 0.007$) concentrations.

These immunofluorescence results show that PFAS exposure altered the tightly regulated MPK-1 activation dynamics in the germline. Because there are different possible causes for these

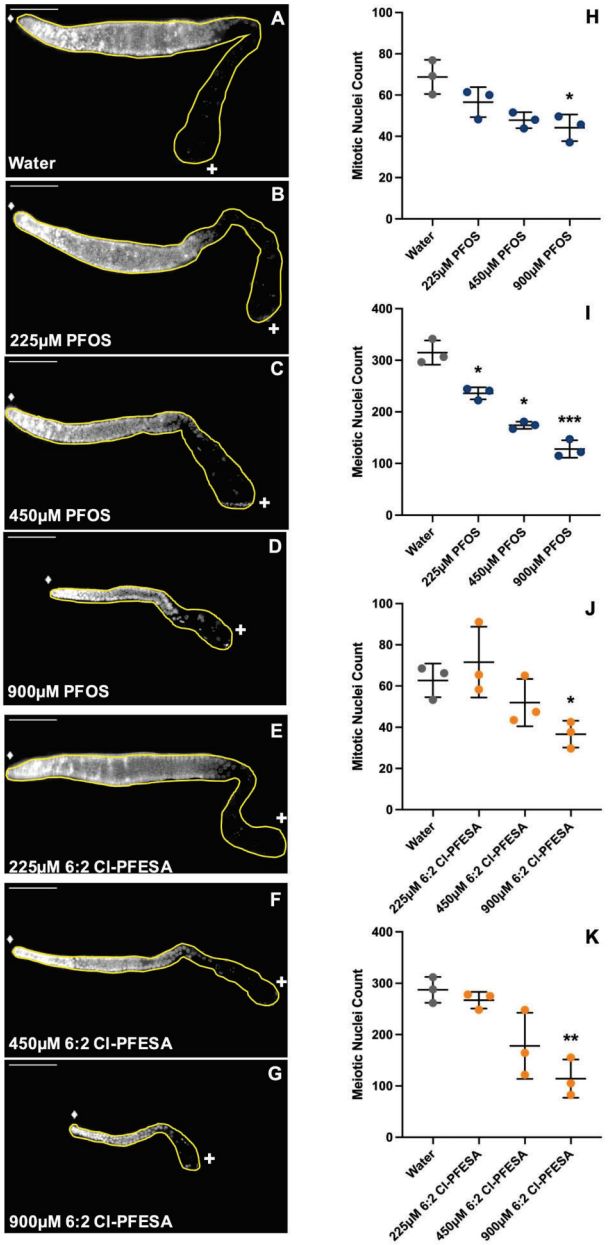

Fig. 3. PFOS or 6:2 Cl-PFESA exposures decrease gonad size with greater impacts on meiotic nuclei than mitotic nuclei. Gonads of adult hermaphrodites unexposed to PFAS (A) exhibit normal size with oogenic germ cell progression through meiosis in a distal (◆) to proximal (✚) orientation. Representative images are shown from *C. elegans* exposed to PFOS (B, C, D) or 6:2 Cl-PFESA (E, F, G). Mitotic nuclei counts were significantly decreased with exposure to NGM treated with 900 µM (H) PFOS or (J) 6:2 Cl-PFESA. Meiotic nuclei counts were significantly decreased with (I) all PFOS exposures and the (K) 900 µM 6:2 Cl-PFESA exposure. Concentrations are reported as the concentrations of solutions applied to solid NGM at a ratio of 1:45 volume to volume. Images show DAPI-stained gonad nuclei in white. Nuclei counts are based on one plane from a single gonad arm per animal. Each point represents the mean nuclei counts from gonads of 6 to 19 (PFOS) or 3 to 14 (6:2 Cl-PFESA) individual *C. elegans* exposed on a single NGM-containing plate. $n = 3$ independent NGM plates per treatment. Error bars represent mean and standard deviation. $^*P < 0.05$, $^{**}P < 0.01$, $^{***}P < 0.001$ (one-way Welch's ANOVA with Dunnett's T3 post hoc). Scale bars = 50 µm.

effects, RNA sequencing was performed next to inform likely pathways involved in inappropriate MPK-1 activation and germline dysfunction.

Gonad-specific RNA-seq analysis reveals reduced expression of genes that negatively regulate MPK-1 activation from 6:2 Cl-PFESA exposure

Because it is a less characterized toxicant compared with PFOS, we focused our in-depth transcriptomic analysis on 6:2 Cl-PFESA. Indeed, a wealth of molecular data are available for PFOS, including whole-animal differential mRNA expression levels for *C. elegans* exposed to PFOS (Stylianou et al. 2019; Yin et al. 2021).

Out of 31,881 mRNA transcript isoforms contained in the WormBase WS287 mRNA transcripts FASTA file, we detected 22,478 isoforms from 15,734 unique genes in at least one of the pooled gonad samples. Based on DESeq2 analysis, 200 mRNA isoforms from 195 unique genes were differentially expressed (Benjamini-Hochberg P-value < 0.05) in 6:2 Cl-PFESA-exposed compared with control worm gonads (Table S1). Of these mRNA isoforms, 115 were significantly upregulated, with 89 increased by more than 1.25-fold, whereas 85 were significantly downregulated, with 26 decreased by less than 0.75-fold (Fig. 6A). By fold-change (FC), the most upregulated genes were those for the UDP-glycosyltransferase UGT-62 (ortholog of human UGT2B4/7/10; FC 3.4), the cytochrome P450 (CYP) enzyme CYP-13A6 (ortholog of human CYP3A4/5/7; FC 2.3), and the cathepsin CPL-1 (ortholog of human CTSL; FC 2.2). The most downregulated genes were those for the splicing factor SWP-1 (ortholog of human SFSWAP; FC 0.05), the exonuclease W02F12.4 (ortholog of human TREX1/2; FC 0.3), and the carbohydrate transmembrane transporter W02D3.4 (ortholog of human TMEM144; FC 0.5).

Among the significantly downregulated genes were 3 involved in the negative regulation of MPK-1 activation: *acs-4* (ortholog of human ACSL3/4; FC 0.93), *nmt-1* (ortholog of human NMT1/2; FC 0.87), and *puf-8* (ortholog of human PUM1/2; FC 0.94) (Fig. 6B). ACS-4 and NMT-1 work in tandem to regulate the MPK-1 phosphatase PPM-2 via gonad fatty acid levels (Tang and Han 2017). Germline fatty acids are supplied from the intestine via gonad sheath–germ cell innexins, and expression of the innexin gene *inx-14* was also significantly downregulated by 6:2 Cl-PFESA exposure (Starich et al. 2020). PUF-8 negatively regulates MPK-1 activation by suppressing mRNA of LET-60 (ortholog of human RAS and activator of MPK-1) (Vaid et al. 2013). A Pumilio family RNA-binding protein (RBP), PUF-8 also promotes mitotic germ cell proliferation, suppression of somatic transcripts, and the switch to oocyte production in conjunction with FBF-1 (Bachorik and Kimble 2005; Ariz et al. 2009; Mainpal et al. 2011).

Gene set enrichment analysis of 6:2 Cl-PFESA-exposed gonads implicates alterations in metabolism and P granule-associated functions

Based on gene set enrichment analysis using PANGEA, upregulated genes were significantly enriched (Benjamini and Hochberg $P < 0.01$, fold enrichment >2) for 15 gene sets (Fig. 6B). Biological process gene sets enriched in upregulated genes included cell death/necrotic cell death, immune system process, metabolic process, and proteolysis. Cell death genes included multiple aspartyl proteases that localize to the lysosome. Immune system genes included lysozymes and other pathogen response genes. Metabolic genes included those involved in carbohydrate and protein metabolism, as well as pyrimidine biosynthesis. Proteolysis genes included multiple cathepsins and peptidases. Cellular component gene sets included lysosome, extracellular region/space, mitochondrial proton-transporting ATP synthase stator stalk, and yolk granule. Molecular function gene sets enriched in upregulated genes included aspartic-type

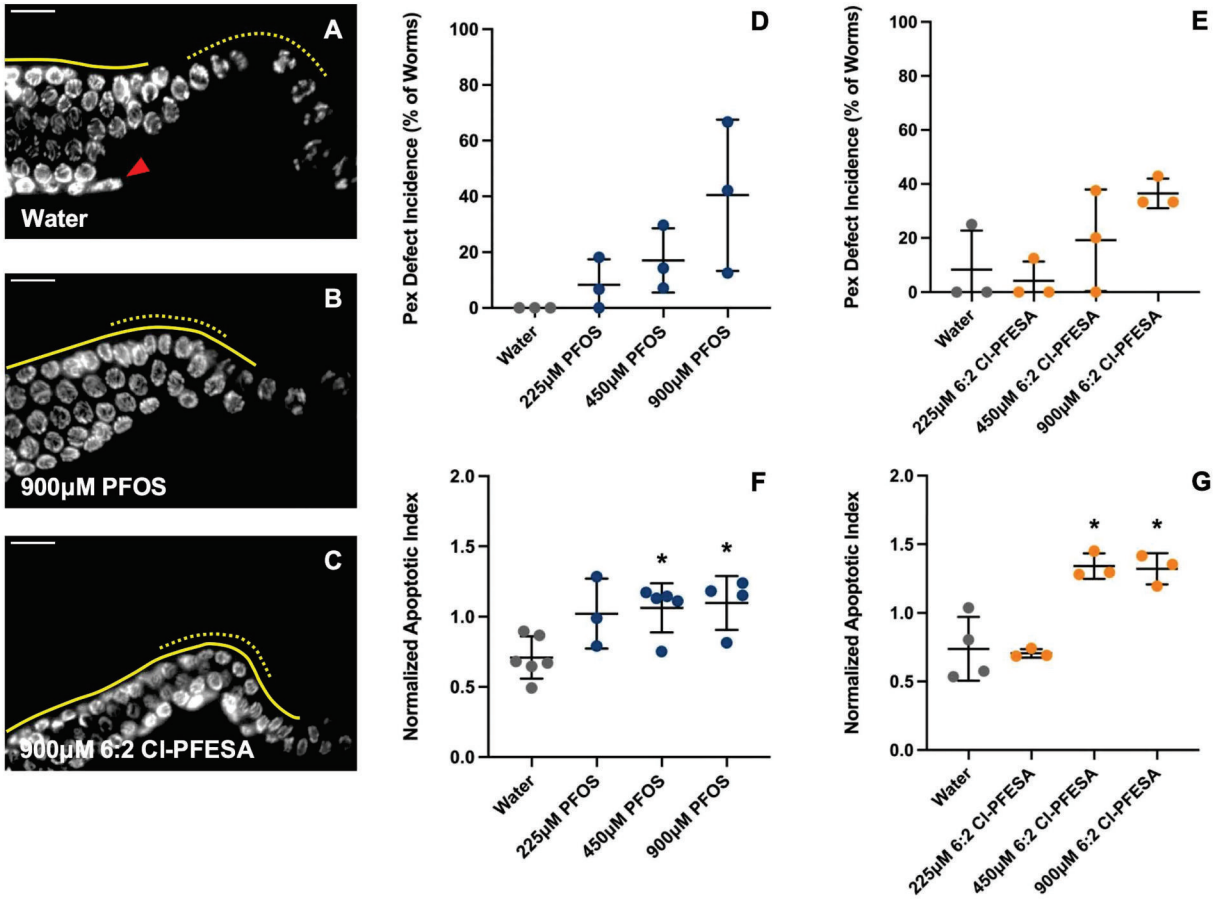

Fig. 4. Defects in pachytene exit coincide with increased apoptosis in late pachytene. A) Nuclei in oogenic *C. elegans* gonads typically transition from pachytene (solid yellow line) to diplotene upon entering the gonad bend (dashed yellow line), as was observed in all but a single control animal. The red arrow points to a gonad sheath cell nucleus. Pachytene exit defect (Pex), where pachytene-stage nuclei extend into and beyond the gonad bend (B and C), was observed at a mean frequency of approximately 35% to 40% in worms exposed to 900 μM (D) PFOS or (E) 6:2 Cl-PFESA. Poisson regression modeling with offset for treatment group size indicated increasing Pex incidence with increasing PFOS or 6:2 Cl-PFESA concentrations. Increased rates of apoptosis relative to the number of pachytene nuclei (i.e. apoptotic index) was also observed with exposure to NGM treated with 450 and 900 μM (F) PFOS or (G) 6:2 Cl-PFESA. Concentrations are reported as the concentrations of solutions applied to solid NGM at a ratio of 1:45 volume to volume. Images show DAPI-stained gonad nuclei in white. Pex incidence was calculated as the percent of gonads exhibiting the Pex phenotype relative to the total number of gonads assessed. For D and E, each point represents Pex incidence out of 7 to 27 (PFOS) or 3 to 15 (6:2 Cl-PFESA) individual *C. elegans* exposed on a single NGM-containing plate. $n = 3$ independent NGM plates per treatment. Apoptotic index was calculated as the ratio of apoptotic nuclei in late pachytene to the average number of pachytene nuclei for a given treatment and was normalized to the mean across all treatment groups within each experimental repeat. For F and G, each point represents the mean apoptotic index from gonads of 15 to 18 (PFOS) or 8 to 20 (6:2 Cl-PFESA) individual *C. elegans* exposed on a single NGM-containing plate. $n = 3$ to 6 independent NGM plates per treatment. Error bars represent mean and standard deviation. *$P < 0.05$ (one-way Welch's ANOVA with Dunnett's T3 post hoc). Scale bars = 10 μm.

endopeptidase activity, peptidase activity, carbohydrate binding, hydrolase activity, and amino acid binding.

Downregulated genes were significantly enriched (Benjamini and Hochberg $P < 0.01$, fold enrichment >2) for 9 gene sets based on PANGEA analysis (Fig. 6C). Biological process gene sets enriched in downregulated genes included negative regulation of phagocytosis and engulfment, protein deglutathionylation, and cellular response to hypoxia. Cellular component gene sets enriched in downregulated genes included cytoplasm and sarcoplasmic reticulum membrane. Molecular function gene sets enriched among downregulated genes included nutrient reservoir activity, lipid transporter activity, protein-glutamine gamma-glutamyltransferase activity, and acetyl-CoA C-acetyltransferase activity.

We further compared differentially expressed genes to published *C. elegans*-specific gene expression data using WormExp v2.0 (Yang et al. 2016). Based on this analysis, genes upregulated in the gonad by 6:2 Cl-PFESA exposure significantly overlapped (Bonferroni $P < 0.05$) with 29 unique gene sets collected from adult hermaphrodite worms (Table S2). Seven of these gene sets (24%) were for genes upregulated in gonads collected from worms with genetically altered or abolished P granules (Fig. 6D). P granules are condensates of RNA and protein essential for germline function that localize to nuclear pores in immature germ cells and are involved in post-transcriptional regulation primarily through inhibiting translation and organizing small RNA pathways (Campbell and Updike 2015; Lev and Rechavi 2020; Chen et al. 2022). Genes upregulated by 6:2 Cl-PFESA exposure also highly overlapped with 7 gene sets (24%) upregulated in worms lacking germ cells, either due to physical ablation of primordial germ cells or genetic mutations in *glp-1* or *glp-4* that lead to temperature-sensitive inhibition of germ cell proliferation, further suggesting disruption of the germ cell-specific program.

Genes downregulated by 6:2 Cl-PFESA exposure significantly overlapped (Bonferroni $P < 0.05$) with 9 gene sets using WormExp v2.0 (Table S2). Two of these gene sets (22%) overlapped with

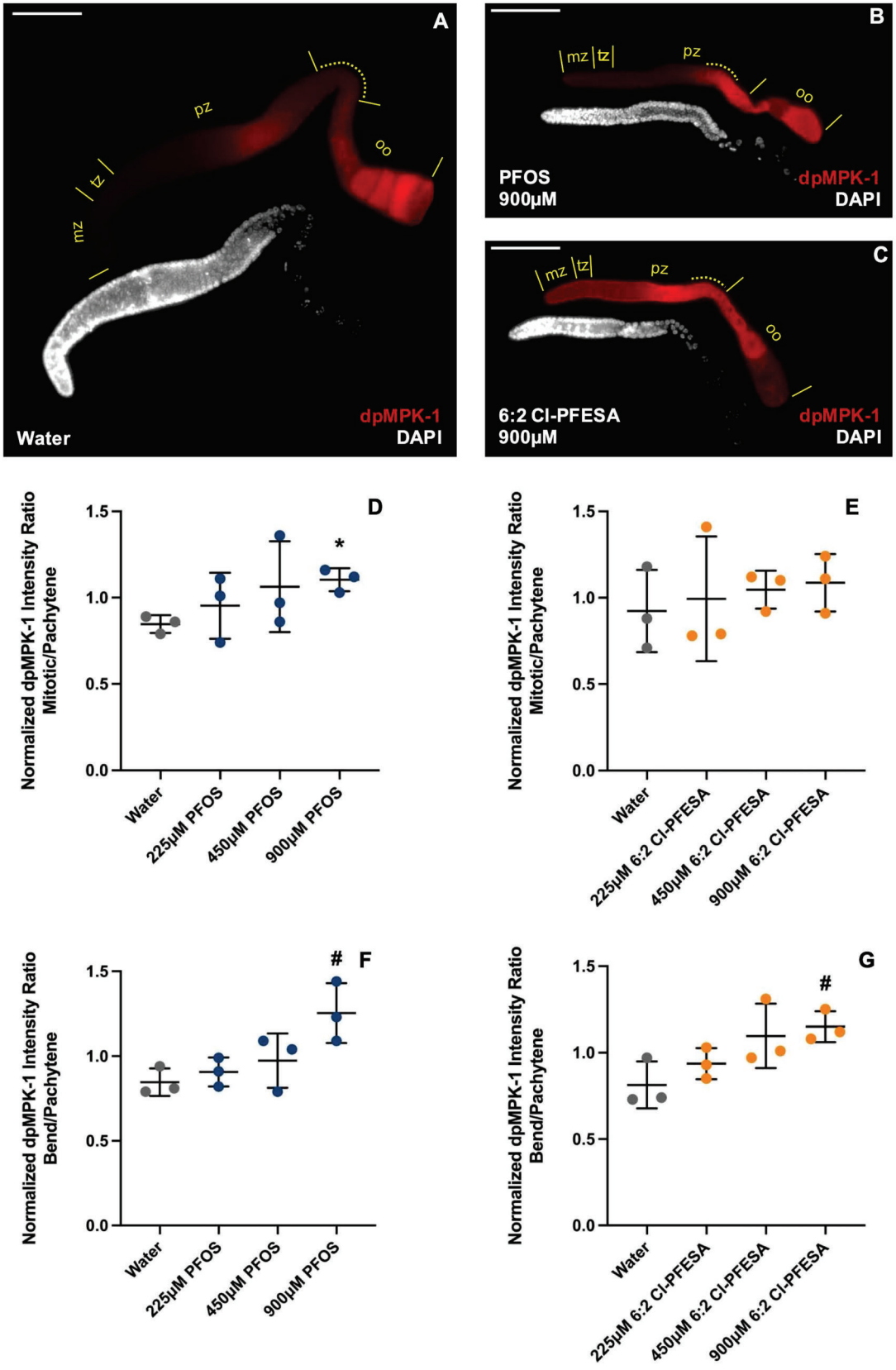

Fig. 5. Aberrant spatial activation of MAP kinase MPK-1 is caused by PFOS and 6:2 Cl-PFESA exposures. A) Oogenic *C. elegans* gonads typically exhibit MPK-1 activation (dpMPK-1, red) in mid to late pachytene zone (pz) and proximal oocytes (oo) with reduced activation in the gonad bend (dashed yellow line) and no activation in the mitotic (mz), transition (tz), or early pachytene zones. Representative images of gonads from worms exposed to NGM treated with 900 µM (B) PFOS or (C) 6:2 Cl-PFESA show spatial changes in MPK-1 activation. Gonads exposed to (D) 900 µM PFOS showed significant increases in dpMPK-1 fluorescence intensity in the mitotic zone relative to pachytene but (E) 6:2 Cl-PFESA exposure did not. Both (F) PFOS and (G) 6:2 Cl-PFESA exposures caused increasing trends in relative dpMPK-1 fluorescence intensity in the gonad bend based on linear regression modeling with

genes downregulated in worms lacking germ cells (Fig. 6E). Additionally, genes downregulated by 6:2 Cl-PFESA exposure significantly overlapped with mRNAs that bind to the RBPs GLD-1 and FBF-1, which act as translational repressors in the germline (Lee et al. 2007a; Kaye et al. 2009; Scheckel et al. 2012). Genes downregulated by 6:2 Cl-PFESA exposure also significantly overlapped with those depleted of sRNAs in *ego-1* or *glp-4* mutants, as well as those with antisense sRNAs that bind to CSR-1 (Table S2). EGO-1 is a germline-expressed RNA-dependent RNA polymerase that generates a class of sRNAs called 22G-RNAs (Seroussi et al. 2023). CSR-1 is an Argonaute protein that binds 22G-RNAs, and 22G-RNAs that bind to CSR-1 are depleted in *glp-4* mutants lacking a germline (Caudy et al. 2003; Claycomb et al. 2009).

Beyond overlapping with RBP-specific gene sets, mRNA of several RBPs was differentially expressed with 6:2 Cl-PFESA exposure (Table S2). Downregulated RBP genes included those for the Tudor-domain proteins TSN-1 and SIMR-1, the K homology domain proteins MINA-1 and FUBL-4, and the Pumilio homology domain protein PUF-8. Upregulated RBP genes included those for the RNA recognition motif protein PBT-1 and the Argonaute proteins WAGO-4 and PPW-2. PUF-8 binds to mRNA, and PTB-1 is involved in splicing (Arribere et al. 2020; Xu et al. 2021). *tsn-1*, *simr-1*, *mina-1*, *fubl-4*, *wago-4*, and *ppw-2* all either genetically or physically interact with sRNAs (Caudy et al. 2003; Haskell and Zinovyeva 2021; Seroussi et al. 2023); *tsn-1* and *fubl-4* interact with miRNAs, whereas *simr-1*, *mina-1*, *wago-4*, and *ppw-2* interact with secondary endogenous small interfering RNAs (endo-siRNAs), including 22G-RNAs (Sendoel et al. 2019; Manage et al. 2020; Seroussi et al. 2023).

Taken together, the gonad-specific mRNA sequencing data indicate that 6:2 Cl-PFESA exposure activates cell death, the innate immune system, and proteolysis while dysregulating carbohydrate and lipid metabolism. Moreover, the data indicate a clear impact of 6:2 Cl-PFESA on RBP networks, particularly those associated with P granules and those involved in post-transcriptional gene regulation and sRNA function.

sRNA-seq shows multiple gonadal sRNA populations altered by 6:2 Cl-PFESA exposure

Because mRNA sequencing results indicated that multiple Argonautes and sRNA-related genes were altered by 6:2 Cl-PFESA exposure, we also performed sRNA sequencing and analysis on the same gonad samples. The *C. elegans* gonad has 4 main classes of sRNAs: piRNA (or 21U-RNA), 22G-RNA, 26G-RNA, and miRNA (Sundby et al. 2021). Different sRNA types associate with specific Argonaute proteins, facilitating different effector functions on target RNAs. Loss-of-function mutants for several Argonautes and sRNA biogenesis proteins exhibit severe germ cell defects or sterility in *C. elegans* (Rechavi and Lev 2017; Sundby et al. 2021).

Transcribed 21U-RNAs/piRNAs associate with the Argonaute PRG-1 in the cytoplasm (Seroussi et al. 2023). Cytoplasmic PRG-1 concentrates in P granules, where it stabilizes and facilitates effector function of 21U-RNAs (Seroussi et al. 2023). Transcripts bound by PRG-1 via guide 21U-RNAs/piRNAs are used to generate 22G-RNAs that promote transcriptional silencing (Sapetschnig et al. 2015). Mean normalized 21U-RNA levels were lower in gonads exposed to 6:2 Cl-PFESA compared with controls within each experimental repeat, but 95% confidence intervals overlapped ($P = 0.08$) (Fig. 7A). DESeq2 analysis did not reveal differential expression of any individual 21U-RNA.

22G-RNAs are endo-siRNAs generated antisense to their transcript targets. 22G-RNAs can have various effector functions depending on the Argonaute pathway with which they associate (Seroussi et al. 2023). In the gonad samples, 22G-RNAs were identified antisense to a total of 14,934 transcript targets (Table S1), similar to the total number of mRNA transcripts detected in the gonad samples. Based on sequencing results, global 22G-RNA levels in gonads were unchanged by 6:2 Cl-PFESA exposure (Fig. 7B). However, DESeq2 analysis revealed 185 significantly upregulated and 99 significantly downregulated (Benjamini-Hochberg $P < 0.05$) 22G-RNA target transcripts (Fig. 7C). Upregulated and downregulated targets of 22G-RNAs were compared with those previously reported to IP with germline-expressed Argonaute proteins to provide more insight into their biological relevance (Seroussi et al. 2023). Based on this analysis, targets of upregulated 22G-RNA were significantly enriched (Bonferroni $P < 0.001$) in those associated with the Argonautes NRDE-3, SAGO-1, PPW-1, HRDE-1, and WAGO-1 (Fig. 7D). NRDE-3 and SAGO-1 are expressed in the somatic gonad and mainly target lncRNAs for silencing (Billi et al. 2014; Seroussi et al. 2023) (Fig. S2A). PPW-1, HRDE-1, and WAGO-1 primarily target protein-coding mRNAs that are normally silenced in the oogenic gonad (Buckley et al. 2012; Seroussi et al. 2023). Among targets of downregulated 22G-RNAs, those associated with the Argonaute PPW-2 were significantly enriched (Bonferroni $P < 0.001$) (Fig. 7D). PPW-2 primarily localizes to P granules in the mitotic/distal region of the adult gonad and targets spermatogenic protein-coding mRNA (Seroussi et al. 2023). Notably, targets of both CSR-1 and WAGO-4 22G-RNAs, which highly overlap with one another and include most constitutively expressed germline genes, were significantly depleted (Bonferroni $P < 0.001$) among targets of 22G-RNAs both upregulated and downregulated by 6:2 Cl-PFESA exposure (Fig. 7D). These data indicate that, although the generation and/or stabilization of constitutively expressed germline 22G-RNAs appears to be largely unaffected by 6:2 Cl-PFESA exposure, somatic and sex-specific 22G-RNAs were significantly altered.

We identified 26G-RNAs for a total of 7,886 transcript targets in the gonad samples. Similar to 22G-RNAs, global 26G-RNA levels did not differ between control and 6:2 Cl-PFESA-exposed gonads (Fig. S2B). Based on DESeq2 analysis, only 9 targets of 26G-RNAs were differentially expressed (Benjamini-Hochberg $P < 0.05$), with 5 upregulated and 4 downregulated (Fig. S2C). All significantly downregulated targets of 26G-RNAs were also significantly downregulated targets of 22G-RNAs. Three of the 5 upregulated targets of 26G-RNAs were also significantly upregulated targets of 22G-RNAs. These data are not surprising given that 22G-RNAs can be generated in response to 26G-RNA targeting (Billi et al. 2014).

We detected 173 miRNAs in the gonad samples. Global miRNA levels did not differ significantly between control and 6:2 Cl-

Fig. 5. Continued
near significant increases ($P < 0.10$) in the highest treatment groups relative to controls. Representative images of single gonad arms are shown with both dpMPK-1 immunofluorescence (red) and DAPI nuclei staining (white) for context. Concentrations are reported as the concentrations of solutions applied to solid NGM at a ratio of 1:45 volume to volume. Relative intensity ratios were normalized to the mean across all treatment groups within each experimental repeat. Each point represents the mean relative intensity ratio from gonads of 7 to 20 (PFOS) or 3 to 15 (6:2 Cl-PFESA) individual *C. elegans* exposed on a single NGM-containing plate. $n = 3$ independent NGM plates per treatment. Error bars represent mean and standard deviation. $^{\#}P < 0.10$, $^{*}P < 0.05$ (one-way Welch's ANOVA with Dunnett's T3 post hoc). Scale bar = 50 μm.

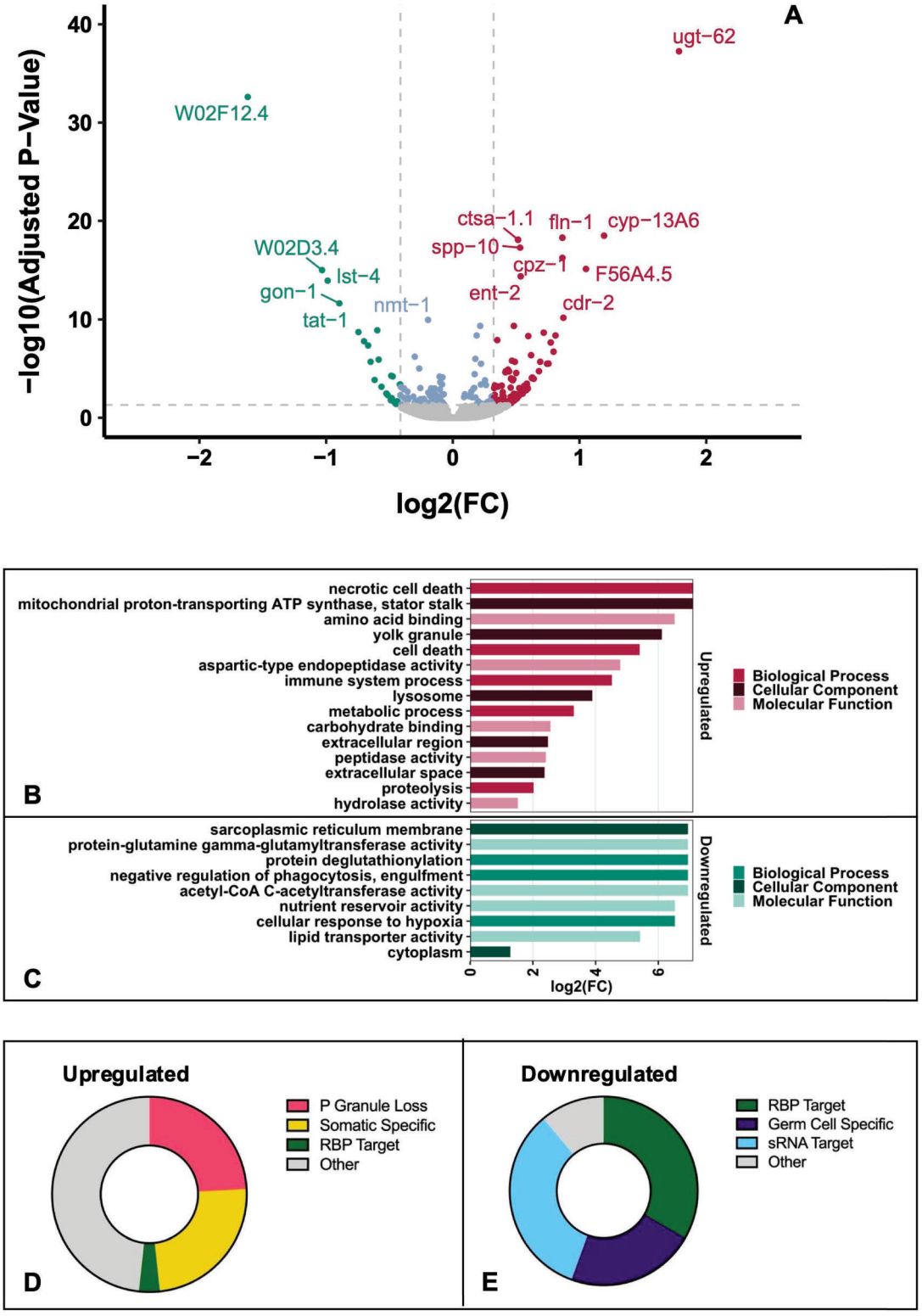

Fig. 6. Shifts in the gonad transcriptome are evident from 6:2 Cl-PFESA exposure. Gonad-specific mRNA sequencing data reveal that worms exposed to NGM treated with 450 μM 6:2 Cl-PFESA exhibited (A) 115 significantly upregulated and 85 significantly downregulated (Benjamini–Hochberg $P < 0.05$) gene isoforms based on differential expression analysis. GO analysis using PANGEA experimental gene sets shows (B) cell death, metabolic, and immune gene sets enriched among upregulated genes and (C) metabolic, enzyme, and lipid transport gene sets enriched among downregulated genes. Gene set enrichment analysis using WormExp showed significant overlap (Bonferroni $P < 0.05$) of (D) upregulated genes with those upregulated by P granule loss or germ cell loss, whereas (E) downregulated genes significantly overlapped with those specific to germ cells as well as small RNA and RBP targets. RNA samples were pooled from gonads of approximately 140 individual *C. elegans* exposed on a single NGM-containing plate. $n = 3$ independent NGM plates per treatment (water or 450 μM 6:2 Cl-PFESA applied to NGM). FC: fold change; RBP: RNA-binding protein. Horizontal dashed line marks Benjamini–Hochberg adjusted *P*-value of 0.05. Vertical dashed lines mark FC 0.75 and 1.25.

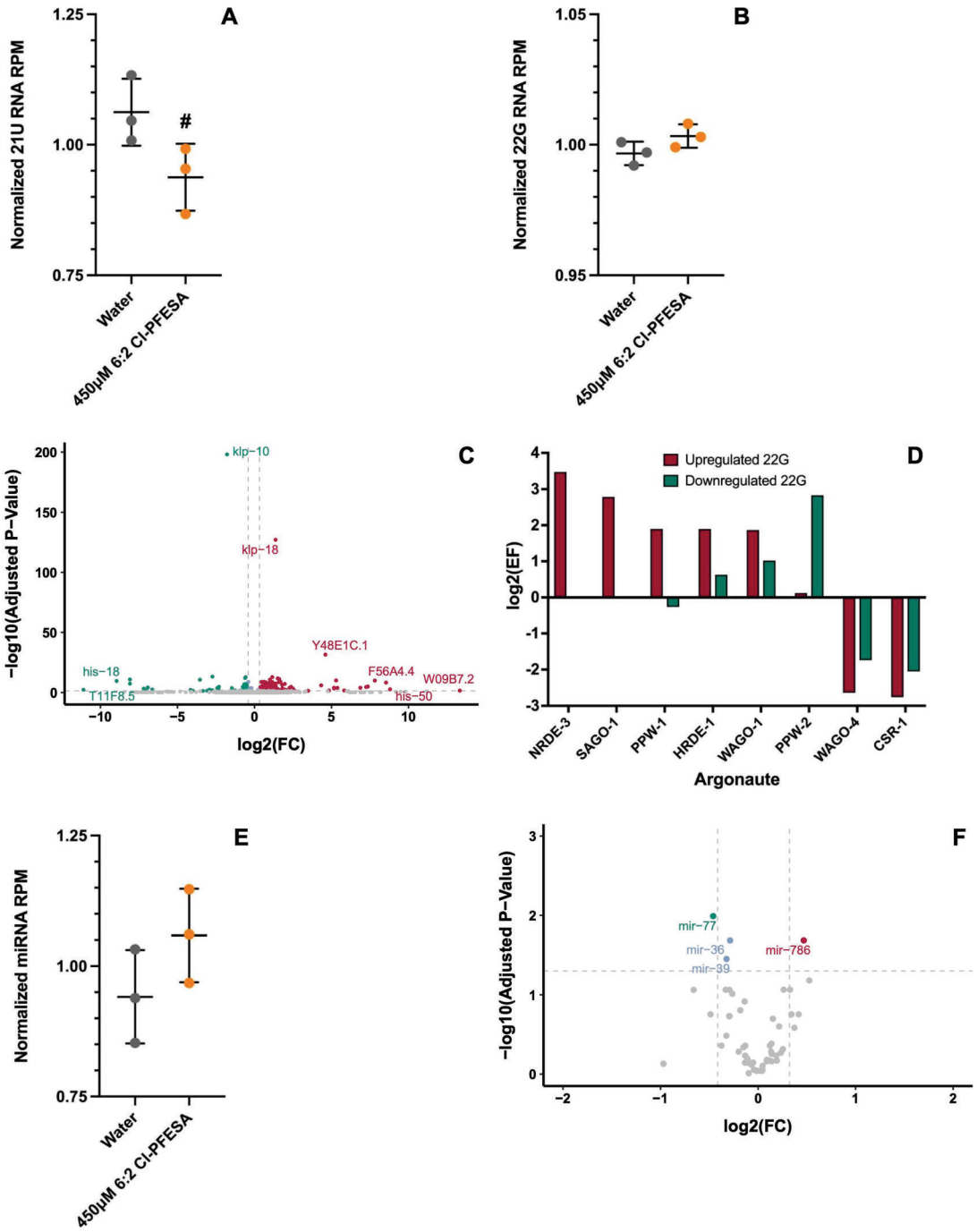

Fig. 7. 6:2 Cl-PFESA exposure alters specific sRNA subpopulations in the oogenic gonad. sRNA sequencing of gonads revealed that (A) mean 21U-RNA/piRNA levels were lower with 6:2 Cl-PFESA and reached near significance ($P < 0.10$). B) Global 22G-RNA levels were not significantly changed by 6:2 Cl-PFESA exposure. C) DESeq2 analysis of 22G-RNAs indicated that 185 targets of 22G-RNAs were significantly upregulated and 99 targets were significantly downregulated (Benjamini–Hochberg $P < 0.05$), as shown in the volcano plot. D) Based on the hypergeometric distribution, targets of upregulated 22G-RNAs were significantly enriched (Bonferroni $P < 0.001$) for those that immunoprecipitate with the Argonautes NRDE-3, SAGO-1, PPW-1, and WAGO-1 based on data from Seroussi et al. 2023. Targets of downregulated 22G-RNAs were significantly enriched (Bonferroni $P < 0.001$) for those that immunoprecipitate with the Argonaute PPW-2. E) Global miRNA levels in gonads did not significantly differ by 6:2 Cl-PFESA exposure. F) One miRNA was significantly upregulated (Benjamini–Hochberg $P < 0.05$) and three miRNAs were significantly downregulated (Benjamini–Hochberg $P < 0.05$) by 6:2 Cl-PFESA exposure, as shown in the volcano plot. sRNA reads were calculated per million genome-mapped reads (excluding sense-mapped reads that likely represent degradation products) and normalized to the mean across treatment groups within each experimental repeat. Concentrations are reported as the concentrations of solutions applied to solid NGM at a ratio of 1:45 volume to volume. RNA samples were pooled from gonads of approximately 140 individual *C. elegans* exposed on a single NGM-containing plate. n = 3 independent NGM plates per treatment. Error bars represent mean and standard deviation. RPM, reads per million; EF, enrichment factor; FC, fold change. Horizontal dashed line marks Benjamini–Hochberg adjusted *P*-value of 0.05. Vertical dashed lines mark FC 0.75 and 1.25.

PFESA-exposed gonads (Fig. 7E). Based on DESeq2 analysis, 4 miRNAs were differentially expressed ($P < 0.05$), with 1 upregulated and 4 downregulated (Fig. 7F). The significantly upregulated miRNA was *miR-786*, which is expressed in gonadal sheath cells, as well as the intestine, and represses fatty-acid elongase ELO-2 (de Lencastre et al. 2010; Kemp et al. 2012). Two of the

significantly downregulated miRNAs were *mir-36* and *mi-39*, which belong to the *mir-35* family. *miR-35* family miRNAs are restricted to the germline and are most strongly expressed in late-pachytene, diplotene, and diakinesis-stage oocytes (McEwen et al. 2016; Minogue et al. 2018). Mutations in *miR-35* family miRNAs cause dysregulation of MPK-1, Pex defects, and reproductive dysfunctions (Minogue et al. 2018; Tran et al. 2019), resembling effects we observed with 6:2 Cl-PFESA and PFOS exposures. The other downregulated miRNA, *mir-77*, is expressed at moderate levels in the gonad but is enriched in the intestine (Diag et al. 2018; Brosnan et al. 2021). *mir-77* mutants exhibit increases in embryonic lethality (Brenner et al. 2010).

Overall, the sRNA sequencing data are consistent with the mRNA sequencing data, indicating that 6:2 Cl-PFESA exposure dysregulates essential gonad genes and differentially affects 22G-RNA populations. In addition, the data point toward dysfunction of processes mediated via P granules, liquid-like biomolecular condensates associated with the nuclear pores of developing germ cell nuclei. Many P granule functions have been shown to be dependent upon proper P granule structure, which can be altered by genetic manipulations, thermal stress, and changes in physicochemical properties. Therefore, it is possible that 6:2 Cl-PFESA exposure could impact gonad functions by altering P granule homeostasis.

6:2 Cl-PFESA and PFOS disrupt P granule structure with ex vivo exposure

As mentioned above, 6:2 Cl-PFESA and PFOS, similar to many other PFAS, are potent surfactants (Buck et al. 2011), and thus, may cause the disruption of various biomolecular condensates, including P granules. To test this hypothesis, we exposed worms with fluorescently labeled PGL-1, a core P granule protein, to PFOS or 6:2 Cl-PFESA both ex vivo and in vivo.

Ex vivo exposure of gonads in a 1:1 M9:water negative control solution did not cause substantial changes in P granule structure (Fig. 8A). Consistent with previous studies by others (Updike et al. 2011), exposure to the positive control solution 5% 1,6-hexanediol resulted in complete dissolution of P granules within 4 min (Fig. 8B). Ex vivo exposure to 450 μM PFOS resulted in a steady decrease in the proportion of pachytene nuclei exhibiting perinuclear granules over the course of 16 min from initial treatment. By 16 min post exposure, the proportion of nuclei with perinuclear granules was significantly reduced to about 47% (95% CI: 7–52; $P = 0.007$) (Fig. 8C and D). Ex vivo exposure to 10 μM PFOS did not cause changes in the number of perinuclear PGL-1 granules but did increase diffuse PGL-1 in the gonad (Fig. 8E).

Ex vivo exposure to 450 μM 6:2 Cl-PFESA produced more rapid and dramatic reductions in perinuclear granules with less than 10% (95% CI: 0–31; $P = 0.0008$) of nuclei exhibiting perinuclear granules by 12 min post exposure (Fig. 8F). By 16 min, nearly all perinuclear granules were completely lost, leaving a diffuse GFP signal in the gonad (Fig. 8G). Results of ex vivo exposure to 10 μM 6:2 Cl-PFESA were similar to 10 μM PFOS exposure (Fig. 8H).

When imaging live animals after in vivo exposures, the PGL-1::GFP reporter strain showed a partially diffuse pattern in a substantial proportion of control worms, likely due to the effects of levamisole. Levamisole is needed to immobilize the worms for live imaging but has previously shown effects on PGL-1::GFP localization (Elaswad et al. 2022). Therefore, we used an alternative PGL-1::RFP reporter strain for in vivo exposures since PGL-1::RFP appeared to maintain normal perinuclear localization in control worms during microscopy imaging. Following 96 h of in vivo PFOS or 6:2 Cl-PFESA exposure starting from embryos, we did not observe consistent changes in PGL-1::RFP granule number, size, or fluorescence intensity in gonads of any of the treatment groups (data not shown).

Although *pgl-1* mRNA levels were not significantly altered by 6:2 Cl-PFESA exposure, we observed evidence from our mRNA and sRNA sequencing data that 6:2 Cl-PFESA exposure could impact the function of the PGL-1 protein. To determine if PFOS or 6:2 Cl-PFESA interacts with pathways controlling P granule homeostasis, we tested whether the partial sterility phenotype of *pgl-1* loss-of-function mutant worms could be enhanced by PFAS exposure. Thus, *pgl-1(bn102)* worms were exposed to PFOS and 6:2 Cl-PFESA. At 20 °C, *pgl-1(bn102)* mutants, which likely have a null *pgl-1* allele, have a reported sterility incidence of approximately 10%, compared with 0% sterility in wild-type worms (Kawasaki et al. 1998). In our hands, *pgl-1(bn102)* mutants exhibited a mean sterility incidence of 3%. Based on Poisson regression with offset for treatment group size, PFOS exposure in *pgl-1(bn102)* mutants caused an increasing trend in sterility incidence with increasing concentration (McFadden pseudo-R^2=0.06, $P = 0.003$) (Fig. S3B). 6:2 Cl-PFESA exposure in *pgl-1(bn102)* mutants did not cause significant effects on sterility.

Ex vivo exposure to PFOS and 6:2 Cl-PFESA led to disruption in P granule structure, but in vivo exposure did not. These differences are likely due to differences in exposure concentrations, with studies of surfactant proteins showing that high concentrations lead to inhibition of LLPS, a key process that drives P granule formation (Sanchez-Burgos et al. 2021). Although the in vivo effects were not strong enough to substantially affect sterility in the *pgl-1(bn102)* mutants, these data suggest that germ cell dysfunction from PFOS or 6:2 Cl-PFESA exposure could be in part mediated by P granules.

PFAS exposure interacts with other germline processes requiring phase separation

Because our results indicated that PFAS exposure altered the structure and function of P granules, we wondered if PFAS exposure could similarly impact other membraneless subcellular structures with liquid-like properties. We chose to focus on the SC, an evolutionarily conserved structure that is essential for proper chromosome segregation during meiosis. Originally thought to be a rigid structure due to its ladder-like appearance under electron microscopy, the SC has more recently been shown to have liquid-crystalline properties, to be highly dynamic throughout meiotic progression, and to be susceptible to destabilization by treatment with 1,6-hexanediol like P granules (Rog et al. 2017). Furthermore, recent evidence also indicates that proper assembly of the SC between homologous chromosomes depends on CSR-1 and lncRNAs (Tabara et al. 2023). To determine if PFOS or 6:2 Cl-PFESA may alter the function of the SC, we examined embryonic lethality in *syp-3(ok758)* partial-rescue (i.e. hypomorphic) worms (strain CA1218), in which a low but detectable level of embryonic lethality has been reported (Rog et al. 2017).

Unexpectedly, in vivo exposure to PFOS or 6:2 Cl-PFESA at all concentrations tested caused dramatic increases in embryonic lethality in the CA1218 partial-rescue strain (Fig. 9A). Exposure to NGM treated with 900 μM PFOS or 6:2 Cl-PFESA caused a mean embryonic lethality of 97% (95% CI: 70–100; $P < 0.0001$) and 95% (95% CI: 69–99; $P < 0.0001$), respectively. Notably, almost half of individual worms in these exposure groups exhibited 100% embryonic lethality and produced no surviving offspring. Although the CA1218 partial-rescue strain exhibits moderately elevated embryonic lethality compared with wild type

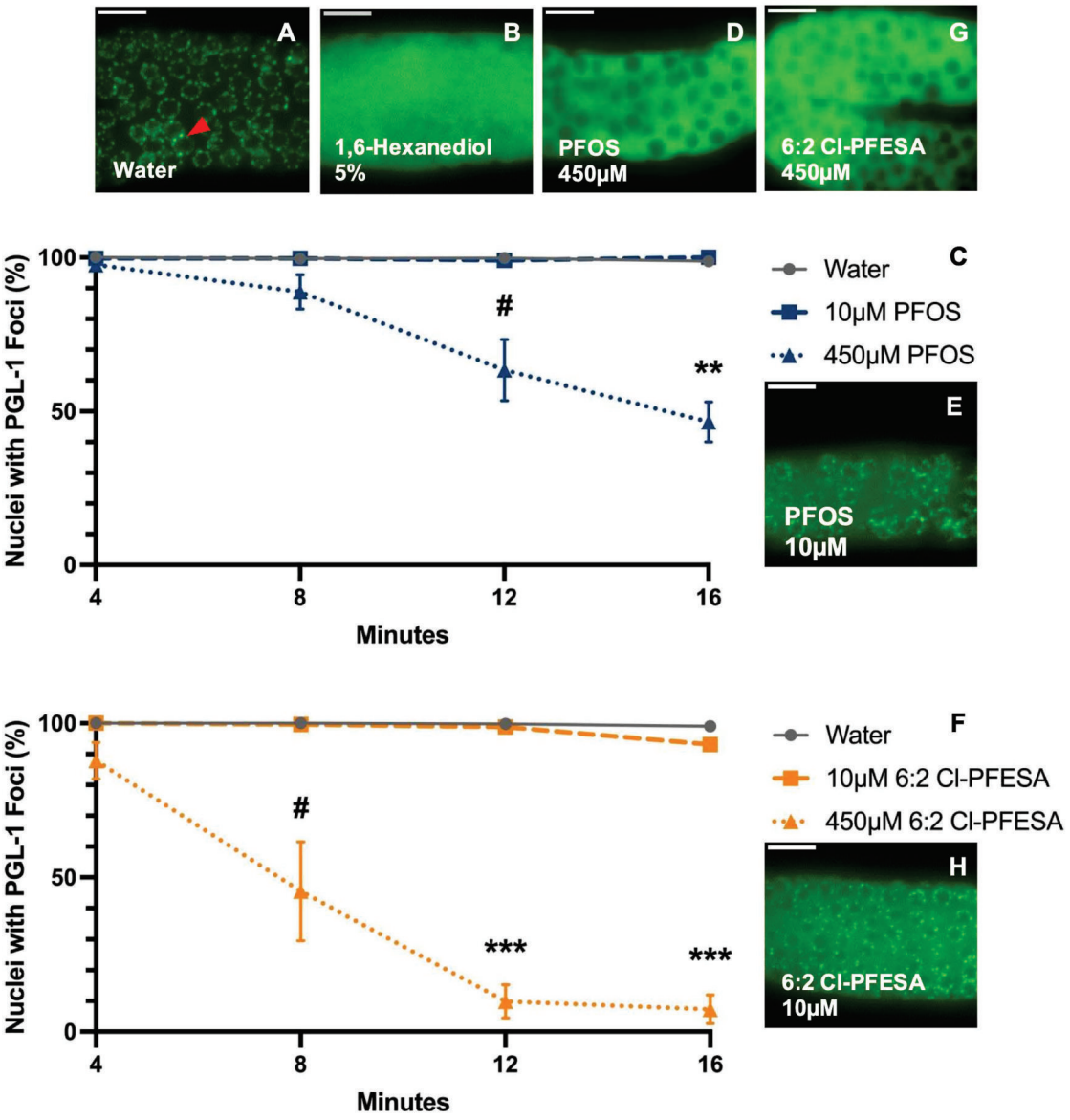

Fig. 8. PFOS and 6:2 Cl-PFESA disrupt P granule structure with ex vivo exposure. A) P granules (red arrow) in the pachytene region of gonads exposed *ex vivo* to 50% M9 in water solution (negative control) maintain their perinuclear, punctate structure for at least 16 min. Ex vivo exposure to (B) 5% 1,6-hexanediol (positive control) causes a complete loss of P granule structure and diffuse PGL-1 in the gonad core. Exposure to (C) 450 µM PFOS leads to approximately 50% of P granules losing their punctate structure after 16 min with diffuse PGL-1 evident (D). Exposure to (C) 10 µM PFOS has no effect at 16 min, though (E) more diffuse PGL-1::GFP is visible compared with controls. Exposure to (F, G) 450 µM 6:2 Cl-PFESA causes near complete loss of punctate P granules by 12 min. Exposure to (F) 10 µM 6:2 Cl-PFESA has no effect on number of punctate at 16 minutes, though (H) more diffuse PGL-1::GFP is visible compared with controls. Representative images of the mid-pachytene region of gonads are shown with PGL-1::GFP in green. Concentrations are reported as final ex vivo exposure concentrations from liquid treatment solutions applied to drops of M9 at a ratio of 1:1 volume to volume. The mean percentage of pachytene nuclei with punctate PGL-1 were assessed from 2 to 4 individual gonads exposed on a single microscope slide per time point. $n = 3$ to 5 independent microscope slides per treatment. Error bars represent mean and standard deviation. $^{\#}P < 0.10$, $^{**}P < 0.01$, $^{***}P < 0.001$ (two-way ANOVA with Dunn post hoc). Scale bar = 15 µm.

(approximately 11% versus <1%), homozygous *syp-3(ok758)* mutants exhibit approximately 95% embryonic lethality (Smolikov et al. 2007). Thus, PFOS and 6:2 Cl-PFESA exposures in the CA1218 strain phenocopied a complete *syp-3* loss-of-function mutation, demonstrating a strong gene–environment interaction.

In the CA1218 strain, the homozygous mutation of the hypomorphic *syp-3(ok758)* allele is partially rescued by a *syp-3::gfp* fusion transgene (Rog et al. 2017). Thus, we monitored in these worms the localization of the GFP-tagged SYP-3 following PFAS exposure. Worms exposed to PFOS or 6:2 Cl-PFESA in vivo did not exhibit obvious changes in SYP-3::GFP localization or structure based on epifluorescence imaging (data not shown). Attempts at ex vivo PFOS or 6:2 Cl-PFESA exposures were inconclusive due to the fast rate of GFP quenching and sensitivity of SYP-3::GFP to disruption under our microscopy conditions. Similarly, we did not observe obvious signs of aneuploidy (i.e. >6 DAPI-stained bodies) at diakinesis (data not shown).

Finally, we monitored the surviving CA1218 broods for male incidence. *C. elegans* with two X chromosomes are hermaphrodites, but chromosome separation errors that result in a single X chromosome generate males. Mean male incidence was slightly

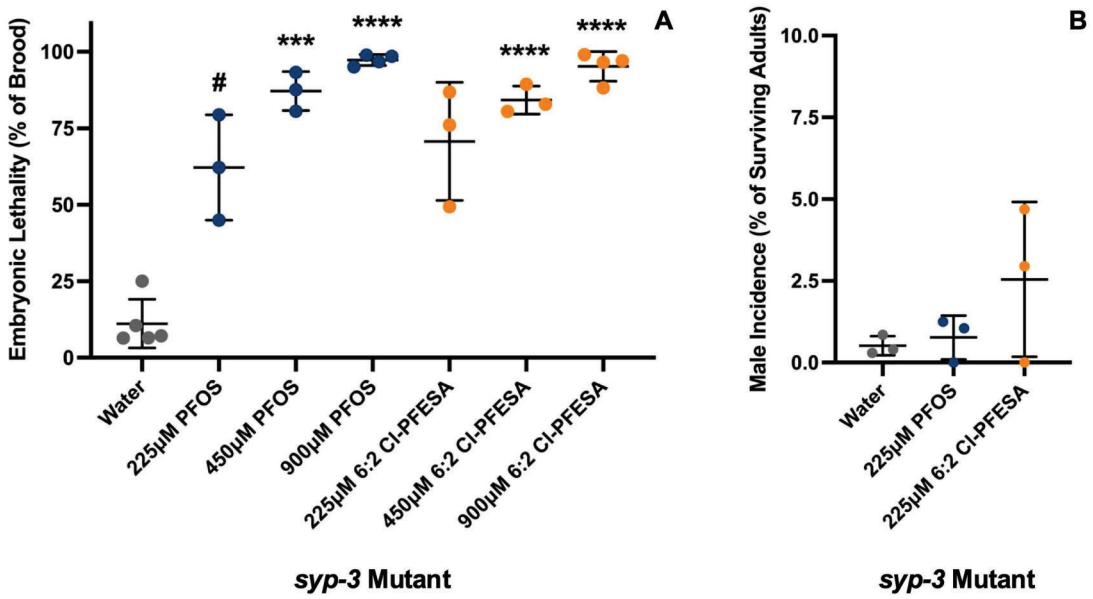

Fig. 9. PFOS or 6:2 Cl-PFESA exposures cause drastic synthetic embryonic lethality in a synaptonemal complex partial-rescue mutant. In the CA1218 *syp-3(ok758)* partial-rescue (PR) strain, where loss of function of the essential synaptonemal complex protein SYP-3 is partially rescued by an extrachromosomal *syp-3::GFP* fusion gene, exposure to solid NGM treated with (A) 450 μM and 900 μM PFOS or 6:2 Cl-PFESA caused significant increases in embryonic lethality. In the 900 μM treatment groups, most worms exhibited complete brood loss (i.e. 100% embryonic lethality). Chromosome separation errors in *C. elegans* lead to the generation of males (XO) instead of hermaphrodites (XX). The mean incidence of males was increased with exposure to (B) 225 μM 6:2 Cl-PFESA, though confidence intervals overlapped with controls. The surviving brood size of the worms exposed to NGM treated with 450 μM and 900 μM PFOS or 6:2 Cl-PFESA was too small (fewer than 20 surviving offspring pooled from 4 to 5 adult worms) to allow for assessment of male incidence in these groups. Concentrations are reported as the concentrations of treatment solutions applied to solid NGM at a ratio of 1:45 volume to volume. Each point represents the mean percent embryonic lethality from the pooled broods of 4 to 5 individual *C. elegans* exposed on each of 4 to 5 NGM-containing plates. $n = 3$ to 5 independent experimental repeats per treatment. Error bars represent mean and standard deviation. $^{\#}P < 0.10$, $^{***}P < 0.001$, $^{****}P < 0.0001$ (one-way Welch's ANOVA with Dunnett's T3 post hoc).

elevated in the CA1218 worms exposed to NGM treated with 225 μM 6:2 Cl-PFESA but did not reach statistical significance (Fig. 9B). However, because the surviving brood size in all PFAS treatment groups was so low, it is possible that the sample size was too small to detect effects on this endpoint.

Although we were unable to determine the exact cause of the drastic increase in embryonic lethality in the CA1218 *syp-3(ok758)* partial-rescue worms exposed to PFAS, it is consistent with our other findings showing negative effects of PFOS and 6:2 Cl-PFESA on meiosis through post-transcriptional and post-translational processes in oogenic germ cells.

Discussion

We have shown that PFOS, and its chlorinated ether analog 6:2 Cl-PFESA, impair germ cell differentiation, reduce the number of functional oocytes, and disrupt reproductive capacity in a dose-dependent manner. Using a systems toxicology approach, we have identified several interacting mechanisms that likely mediate these negative effects, with a key focus on post-transcriptional regulatory networks.

We propose that PFAS, based on their surfactant characteristics, disrupt the assembly and/or maintenance of subcellular structures that rely on phase separation, including P granules and the SC. Assembly and maintenance of phase-separated structures depend on weak intermolecular forces between proteins and RNAs, including hydrophobic and electrostatic interactions. As anionic surfactants, PFOS and 6:2 Cl-PFESA have the potential to alter the thermodynamic favorability of protein–protein and RNA–protein interactions and biomolecular partitioning into the bulk versus condensed phase. Additionally, anionic PFAS have previously been shown to alter secondary protein structure (Prieto et al. 2004; Messina et al. 2007; Wang et al. 2016), which could further change the accessibility of charged or hydrophobic residues and their intermolecular interactions. With both in vivo and ex vivo exposures, PFOS and 6:2 Cl-PFESA appear to exhibit effects similar to those we observed with exposure to 1,6-hexanediol, which disrupts P granules and the SC and causes embryonic lethality (Lemmens and Tijsterman 2011; Updike et al. 2011; Zhang et al. 2020; Liu et al. 2021; Jones and Forsburg 2023; Gombás and Villányi 2024; Neves et al. 2025).

Our mRNA sequencing data show that 6:2 Cl-PFESA exposure caused a shift in the gonad transcriptional profile toward one that resembles worms lacking P granules or lacking germ cells entirely. Consistent with these mRNA data, expression of oocyte-enriched miRNAs of the *miR-35* family was also significantly reduced by 6:2 Cl-PFESA exposure. 22G-RNAs associated with Argonaute proteins involved in somatic gene silencing pathways, as well as those involved in sex-specific germline gene silencing, were significantly increased, further suggesting dysregulation of the germ cell program via sRNAs. In addition, 6:2 Cl-PFESA exposure downregulated mRNA expression of the Pumilio RBP PUF-8, which promotes mitotic germ cell proliferation and suppression of somatic transcripts (Bachorik and Kimble 2005; Ariz et al. 2009; Mainpal et al. 2011). mRNA of germ cell-specific RBPs MINA-1, PPW-2, and WAGO-2 were also differentially expressed. These RBPs act as part of a regulon that impacts germ cell apoptosis and brood size (Sendoel et al. 2019). All in all, these data show negative effects of 6:2 Cl-PFESA on the post-transcriptional gene regulation processes essential for maintaining totipotency and germ cell identity (Ciosk et al. 2006; Knutson et al. 2017).

Our mRNA sequencing data also suggest potential germ cell-autonomous and non-autonomous pathways by which 6:2 Cl-PFESA exposure could cause the observed misactivation of MPK-1 in the gonad. Downregulation of *inx-14*, *acs-4*, and *nmt-1* suggests impaired fatty acid transport from the soma to the gonad may play a role. Germline fatty acids are supplied from the intestine via gonad sheath–germ cell innexins, including INX-14 (Starich et al. 2020). The reduced transcript expression of the acyl-CoA synthetase *acs-4* and the N-myristoyltransferase *nmt-1* suggests that decreased transport of fatty acids from the soma into the gonad could lead to reductions in protein myristoylation. NMT-1 specifically catalyzes the myristoylation of the phosphatase PPM-2, which is necessary for it to deactivate MPK-1 (Tang and Han 2017). *acs-4* loss-of-function mutants exhibit high levels of dpMPK-1 and fail to initiate oogenesis (Tang and Han 2017). Additionally, the downregulation of *miR-35* expression in germ cells could lead to reduced translational suppression of the kinase NDK-1, which promotes MPK-1 activation and germ cell apoptosis in response to stress (Tran et al. 2019). *miR-35–41 (nDf50)* mutants further exhibit Pex defects as well as reduced numbers of oocytes and smaller brood size (Minogue et al. 2018). Downregulation of *puf-8* in the gonad could also contribute to MPK-1 misactivation since PUF-8 suppresses mRNA of LET-60 (a Ras ortholog and activator of MPK-1) (Vaid et al. 2013). These data further support the conclusion that 6:2 Cl-PFESA exposure causes germ cell and reproductive defects through post-transcriptional and post-translational mechanisms that may be rooted in P granule dysfunction.

Our observations that ex vivo exposures to PFAS almost completely disrupted P granule structure, whereas in vivo exposures did not, could be explained by relative PFAS concentrations. In biological contexts with proteins that can act as surfactants, a low surfactant to non-surfactant protein ratio allows for growth and stabilization of phase-separated droplets (Sanchez-Burgos et al. 2021). This scenario appears comparable to our in vivo exposures, where internal PFAS concentrations were likely relatively low. In contrast, a high surfactant-to-non-surfactant protein ratio can completely abrogate phase separation (Sanchez-Burgos et al. 2021). This scenario appears comparable to our ex vivo exposures, where gonads were in direct contact with PFAS solutions and P granule structure was nearly completely disrupted. Even without dissolution of P granules, stabilization of P granules at lower PFAS concentrations could still impair P granule function by altering the dynamics of proteins and RNA partitioning between granules and the bulk cytoplasm.

To the best of our knowledge, this is the first study to examine the potential effects of PFAS exposure on phase separation and functional consequences in living organisms. Other physicochemical effects of PFAS exposure on cellular components have been examined. For example, it has been proposed that increases in membrane fluidity and permeability are key events in male reproductive toxicity from PFAS (Lu et al. 2023). However, many studies have focused on receptor-mediated mechanisms of PFAS health effects, particularly peroxisome proliferator-activated receptors (PPARs) (Evans et al. 2022). Interestingly, heterodimers of PPARβ and retinoid X receptor undergo phase separation at PPAR response elements to promote transcription of target genes (Li et al. 2022). Therefore, it is possible that alterations in phase separation contribute to receptor-mediated effects of PFAS exposure.

Although our study is strengthened by the multiple lines of evidence we present, it also has limitations. A significant limitation is that we do not know the internal doses that resulted from the external exposures to high PFOS or 6:2 Cl-PFESA levels. Gonad-specific measurement of these PFAS would be infeasible given the small mass of *C. elegans* gonads. Others have measured whole-worm PFAS concentrations following feeding with PFAS-treated bacteria, which is similar to our exposure scenario (Stylianou et al. 2019). When fed bacteria incubated in 25 μM PFOS, worms had a whole-body concentration of 4 ng/g (Stylianou et al. 2019). We expect that our exposures resulted in similar concentrations given the 1:45 volume-for-volume dilution of our treatment solutions on solid NGM and the primary route of exposure being ingestion.

This study points to a potential novel mechanism of action of PFAS: Alterations of biomolecular condensates leading to transcriptional and functional impacts on germ cell function. Since the 1950s, thousands of different PFAS have been synthesized by humans and incorporated broadly into industrial processes and consumer products due to their physicochemical characteristics, including high thermal and oxidative stability and low surface tension (Berger et al. 2011). However, while these properties make PFAS desirable commercially, our work and that of others suggest that they may also underlie the impacts of PFAS on fundamental biophysical and chemical properties of living systems (Salwiczek et al. 2012). Effects on protein–protein and protein–RNA interactions should be examined further in future toxicological investigations of PFAS.

Acknowledgments

We thank Dr Lisa Truong for helping with immunofluorescence methodology and general *C. elegans* culturing; Dr Roxane Verdikt for helping with RNA purification and for providing feedback on a previous draft of this manuscript; the lab of Dr Oded Rechavi for sharing their sRNA extraction and purification methods; and the UCLA Technology Center for Genomics & Bioinformatics for performing the library preparation and sequencing of RNA samples.

Supplementary material

Supplementary material is available at *Toxicological Sciences* online.

Funding

APB and ML were supported by the National Institute of Health/National Institute of Environmental Health Sciences Molecular Toxicology Training Program T32ES015457. PA is supported by National Institute of Environmental Health Sciences R01ES027487 and R01ES034251, the John Templeton Foundation, and the Burroughs Wellcome Innovation in Regulatory Science Award. Some strains were provided by the CGC, which is funded by NIH Office of Research Infrastructure Programs (P40 OD010440).

Conflicts of interest. None declared.

References

Achache H, Laurent L, Hecker-Mimoun Y, Ishtayeh H, Rappaport Y, Kroizer E, Colaiácovo MP, Tzur YB. 2019. Progression of meiosis is coordinated by the level and location of MAPK activation via OGR-2 in *Caenorhabditis elegans*. Genetics. 212:213–229.

Allard P, Kleinstreuer NC, Knudsen TB, Colaiácovo MP. 2013. A *C. elegans* screening platform for the rapid assessment of chemical

disruption of germline function. Environ Health Perspect. 121:717–724.
Aparicio-Puerta E, Gómez-Martín C, Giannoukakos S, Medina JM, Scheepbouwer C, García-Moreno A, Carmona-Saez P, Fromm B, Pegtel M, Keller A, *et al.* 2022. sRNAbench and sRNAtoolbox 2022 update: accurate miRNA and sncRNA profiling for model and non-model organisms. Nucleic Acids Res. 50:W710–W717.
Ariz M, Mainpal R, Subramaniam K. 2009. *C. elegans* RNA-binding proteins PUF-8 and MEX-3 function redundantly to promote germline stem cell mitosis. Dev Biol. 326:295–304.
Arribere JA, Kuroyanagi H, Hundley HA. 2020. mRNA editing, processing and quality control in *Caenorhabditis elegans*. Genetics. 215:531–568.
Bachorik JL, Kimble J. 2005. Redundant control of the *Caenorhabditis elegans* sperm/oocyte switch by PUF-8 and FBF-1, two distinct PUF RNA-binding proteins. Proc Natl Acad Sci U S A. 102:10893–10897.
Berger R, Resnati G, Metrangolo P, Weber E, Hulliger J. 2011. Organic fluorine compounds: a great opportunity for enhanced materials properties. Chem Soc Rev. 40:3496–3508.
Bil W, Zeilmaker MJ, Bokkers BGH. 2022. Internal relative potency factors for the risk assessment of mixtures of per- and polyfluoroalkyl substances (PFAS) in human biomonitoring. Environ Health Perspect. 130:77005. https://doi.org/10.1289/ehp10009.
Billi AC, Fischer SEJ, Kim JK. 2014. Endogenous RNAi pathways in *C. elegans*. WormBook. 1–49. https://doi.org/10.1895/wormbook.1.170.1
Brenner JL, Jasiewicz KL, Fahley AF, Kemp BJ, Abbott AL. 2010. Loss of individual MicroRNAs causes mutant phenotypes in sensitized genetic backgrounds in *C. elegans*. Curr Biol. 20:1321–1325.
Brosnan CA, Palmer AJ, Zuryn S. 2021. Cell-type-specific profiling of loaded miRNAs from *Caenorhabditis elegans* reveals spatial and temporal flexibility in Argonaute loading. Nat Commun. 12:2194–2116.
Buck RC, Franklin J, Berger U, Conder JM, Cousins IT, de Voogt P, Jensen AA, Kannan K, Mabury SA, van Leeuwen SPJ. 2011. Perfluoroalkyl and polyfluoroalkyl substances in the environment: terminology, classification, and origins. Integr Environ Assess Manag. 7:513–541.
Buckley BA, Burkhart KB, Gu SG, Spracklin G, Kershner A, Fritz H, Kimble J, Fire A, Kennedy S. 2012. A nuclear Argonaute promotes multigenerational epigenetic inheritance and germline immortality. Nature. 489:447–451.
Calafat AM, Kato K, Hubbard K, Jia T, Botelho JC, Wong L-Y. 2019. Legacy and alternative per- and polyfluoroalkyl substances in the U.S. general population: paired serum-urine data from the 2013–2014 National Health and Nutrition Examination Survey. Environ Int. 131:105048.
Camacho J, Truong L, Kurt Z, Chen Y-W, Morselli M, Gutierrez G, Pellegrini M, Yang X, Allard P. 2018. The memory of environmental chemical exposure in *C. elegans* is dependent on the Jumonji demethylases jmjd-2 and jmjd-3/utx-1. Cell Rep. 23:2392–2404.
Campbell AC, Updike DL. 2015. CSR-1 and P granules suppress sperm-specific transcription in the *C. elegans* germline. Development. 142:1745–1755.
Caudy AA, Ketting RF, Hammond SM, Denli AM, Bathoorn AMP, Tops BBJ, Silva JM, Myers MM, Hannon GJ, Plasterk RHA. 2003. A micrococcal nuclease homologue in RNAi effector complexes. Nature. 425:411–414.
Centers for Disease Control and Prevention. 2018. National Health and Nutrition Examination Laboratory Data 2017–2018. Hyattsville (MD): U.S. Department of Health and Human Services, Centers for Disease Control and Prevention [accessed 2025 Apr 24]. https://wwwn.cdc.gov/nchs/nhanes/search/datapage.aspx?Component=Laboratory&CycleBeginYear=2017.
Chen F, Wei C, Chen Q, Zhang J, Wang L, Zhou Z, Chen M, Liang Y. 2018. Internal concentrations of perfluorobutane sulfonate (PFBS) comparable to those of perfluorooctane sulfonate (PFOS) induce reproductive toxicity in *Caenorhabditis elegans*. Ecotoxicol Environ Saf. 158:223–229.
Chen J, Miao Y, Gao Q, Cui Z, Xiong B. 2021. Exposure to perfluorooctane sulfonate in vitro perturbs the quality of porcine oocytes via induction of apoptosis. Environ Pollut. 284:117508.
Chen W, Brown JS, He T, Wu W-S, Tu S, Weng Z, Zhang D, Lee H-C. 2022. GLH/VASA helicases promote germ granule formation to ensure the fidelity of piRNA-mediated transcriptome surveillance. Nat Commun. 13:5306. https://doi.org/10.1038/s41467-022-32880-2. http://dx.doi.org/10.1038/s41467-022-32880-2.
Chen Y, Panter B, Hussain A, Gibbs K, Ferreira D, Allard P. 2019. BPA interferes with StAR-mediated mitochondrial cholesterol transport to induce germline dysfunctions. Reprod Toxicol. 90:24–32.
Chen Y, Shu L, Qiu Z, Lee DY, Settle SJ, Que Hee S, Telesca D, Yang X, Allard P. 2016. Exposure to the BPA-substitute bisphenol S causes unique alterations of germline function. PLoS Genet. 12: e1006223. https://doi.org/10.1371/journal.pgen.1006223.
Church DL, Guan K-L, Lambie EJ. 1995. Three genes of the MAP kinase cascade, mek-2, mpk-1/sur-1 and let-60 ras, are required for meiotic cell cycle progression in *Caenorhabditis elegans*. Development. 121:2525–2535.
Ciosk R, DePalma M, Priess JR. 2006. Translational regulators maintain totipotency in the *Caenorhabditis elegans* germline. Science. 311:851–853.
Clark KL, George JW, Davis JS. 2024. Adolescent exposure to a mixture of per- and polyfluoroalkyl substances (PFAS) depletes the ovarian reserve, increases ovarian fibrosis, and alters the Hippo pathway in adult female mice. Toxicol Sci. 202:36–49.
Claycomb JM, Batista PJ, Pang KM, Gu W, Vasale JJ, van Wolfswinkel JC, Chaves DA, Shirayama M, Mitani S, Ketting RF, *et al.* 2009. The argonaute CSR-1 and its 22G-RNA cofactors are required for holocentric chromosome segregation. Cell. 139:123–134.
Das D, Arur S. 2017. Conserved insulin signaling in the regulation of oocyte growth, development, and maturation. Mol Reprod Dev. 84:444–459.
Das D, Chen S-Y, Arur S. 2020. ERK phosphorylates chromosomal axis component HORMA domain protein HTP-1 to regulate oocyte numbers. Sci Adv. 6:eabc5580. https://doi.org/10.1126/sciadv.abc5580.
De Felici M, Klinger FG, Farini D, Scaldaferri ML, Iona S, Lobascio M. 2005. Establishment of oocyte population in the fetal ovary: primordial germ cell proliferation and oocyte programmed cell death. Reprod Biomed Online. 10:182–191.
de Lencastre A, Pincus Z, Zhou K, Kato M, Lee SS, Slack FJ. 2010. MicroRNAs both promote and antagonize longevity in *C. elegans*. Curr Biol. 20:2159–2168.
Department of Health and Human Services, Centers for Disease Control and Prevention. 2022. National Report on Human Exposure to Environmental Chemicals. National Health and Nutrition Examination Survey (U.S.) [accessed 2025 Apr 24]. https://stacks.cdc.gov/view/cdc/133100.
Diag A, Schilling M, Klironomos F, Ayoub S, Rajewsky N. 2018. Spatiotemporal m(i)RNA architecture and 3′ UTR regulation in the *C. elegans* germline. Dev Cell. 47:785–800.e8.
Ding N, Harlow SD, Randolph JF Jr, Loch-Caruso R, Park SK. 2020. Perfluoroalkyl and polyfluoroalkyl substances (PFAS) and their effects on the ovary. Hum Reprod Update. 26:724–752.

Domínguez A, Salazar Z, Arenas E, Betancourt M, Ducolomb Y, González-Márquez H, Casas E, Teteltitla M, Bonilla E. 2016. Effect of perfluorooctane sulfonate on viability, maturation and gap junctional intercellular communication of porcine oocytes in vitro. Toxicol In Vitro. 35:93–99.

Droge STJ. 2019. Membrane–water partition coefficients to aid risk assessment of perfluoroalkyl anions and alkyl sulfates. Environ Sci Technol. 53:760–770.

Elaswad MT, Munderloh C, Watkins BM, Sharp KG, Breton E, Schisa JA. 2022. Imaging-associated stress causes divergent phase transitions of RNA-binding proteins in the *Caenorhabditis elegans* germ line. G3 (Bethesda). 12:jkac172. https://doi.org/10.1093/g3journal/jkac172.

Evans N, Conley JM, Cardon M, Hartig P, Medlock-Kakaley E, Gray LE Jr. 2022. In vitro activity of a panel of per- and polyfluoroalkyl substances (PFAS), fatty acids, and pharmaceuticals in peroxisome proliferator-activated receptor (PPAR) alpha, PPAR gamma, and estrogen receptor assays. Toxicol Appl Pharmacol. 449:116136.

Feng J, Soto-Moreno EJ, Prakash A, Balboula AZ, Qiao H. 2023. Adverse PFAS effects on mouse oocyte in vitro maturation are associated with carbon-chain length and inclusion of a sulfonate group. Cell Prolif. 56:e13353. https://doi.org/10.1111/cpr.13353.

Fenton SE, Ducatman A, Boobis A, DeWitt JC, Lau C, Ng C, Smith JS, Roberts SM. 2021. Per- and polyfluoroalkyl substance toxicity and human health review: current state of knowledge and strategies for informing future research. Environ Toxicol Chem. 40:606–630.

Ge W, Li L, Dyce PW, De Felici M, Shen W. 2019. Establishment and depletion of the ovarian reserve: physiology and impact of environmental chemicals. Cell Mol Life Sci. 76:1729–1746.

Gebbink WA, Bossi R, Rigét FF, Rosing-Asvid A, Sonne C, Dietz R. 2016. Observation of emerging per- and polyfluoroalkyl substances (PFASs) in Greenland marine mammals. Chemosphere. 144:2384–2391.

Gervaise AL, Arur S. 2016. Spatial and temporal analysis of active ERK in the *C. elegans* germline. JoVE. 117:54901. https://doi.org/10.3791/54901 [accessed 2025 Jul 20]. https://app.jove.com/t/54901.

Gombás BG, Villányi Z. 2024. 1,6-Hexanediol is inducing homologous recombination by releasing BLM from assemblysomes in *Drosophila melanogaster*. IJMS. 25:1611.

Haskell D, Zinovyeva A. 2021. KH domain containing RNA-binding proteins coordinate with microRNAs to regulate *Caenorhabditis elegans* development. G3 (Bethesda). 11:jkab013. https://doi.org/10.1093/g3journal/jkab013.

He Y, Lv D, Li C, Liu X, Liu W, Han W. 2022. Human exposure to F-53B in China and the evaluation of its potential toxicity: an overview. Environ Int. 161:107108.

Heuvel JPV, Kuslikis BI, Van Rafelghem MJ, Peterson RE. 1991. Tissue distribution, metabolism, and elimination of perfluorooctanoic acid in male and female rats. J Biochem Toxicol. 6:83–92.

Hu Y, Comjean A, Attrill H, Antonazzo G, Thurmond J, Chen W, Li F, Chao T, Mohr SE, Brown NH, *et al.* 2023. PANGEA: a new gene set enrichment tool for *Drosophila* and common research organisms. Nucleic Acids Res. 51:W419–W426.

Index of/releases/WS287/species/c_elegans/PRJNA13758. [accessed 2023 Aug 16]. https://downloads.wormbase.org/releases/WS287/species/c_elegans/PRJNA13758/.

Jones CE, Forsburg SL. 2023. Impact of 1,6-hexanediol on *Schizosaccharomyces pombe* genome stability. G3: Genes, Genomes, Genetics. 13:jkad123.

Kaboré HA, Vo Duy S, Munoz G, Méité L, Desrosiers M, Liu J, Sory TK, Sauvé S. 2018. Worldwide drinking water occurrence and levels of newly-identified perfluoroalkyl and polyfluoroalkyl substances. Sci Total Environ. 616-617:1089–1100.

Kawasaki I, Shim Y-H, Kirchner J, Kaminker J, Wood WB, Strome S. 1998. PGL-1, a predicted RNA-binding component of germ granules, is essential for fertility in *C. elegans*. Cell. 94:635–645.

Kaye JA, Rose NC, Goldsworthy B, Goga A, L'Etoile ND. 2009. A 3′UTR pumilio-binding element directs translational activation in olfactory sensory neurons. Neuron. 61:57–70.

Kemp BJ, Allman E, Immerman L, Mohnen M, Peters MA, Nehrke K, Abbott AL. 2012. miR-786 regulation of a fatty-acid elongase contributes to rhythmic calcium-wave initiation in *C. elegans*. Curr Biol. 22:2213–2220.

Killian DJ, Hubbard EJA. 2005. *Caenorhabditis elegans* germline patterning requires coordinated development of the somatic gonadal sheath and the germ line. Dev Biol. 279:322–335.

Knutson AK, Egelhofer T, Rechtsteiner A, Strome S. 2017. Germ granules prevent accumulation of somatic transcripts in the adult *Caenorhabditis elegans* germline. Genetics. 206:163–178.

Lai KP, Lee JC-Y, Wan HT, Li JW, Wong AY-M, Chan TF, Oger C, Galano J-M, Durand T, Leung KS, *et al.* 2017. Effects of in utero PFOS exposure on transcriptome, lipidome, and function of mouse testis. Environ Sci Technol. 51:8782–8794.

Lancaster C, Zavagno G, Groombridge J, Raimundo A, Weinkove D, Hawkins T, Robson J, Goldberg MW. 2022. Imaging fluorescent nuclear pore complex proteins in *C. elegans*. In: Goldberg MW, editor. Methods in molecular biology. New York (NY): Springer US. p. 373–393.

Leacock SW, Reinke V. 2006. Expression profiling of MAP kinase–mediated meiotic progression in *Caenorhabditis elegans*. PLoS Genet. 2:e174.

Lee M-H, Hook B, Pan G, Kershner AM, Merritt C, Seydoux G, Thomson JA, Wickens M, Kimble J. 2007a. Conserved regulation of MAP kinase expression by PUF RNA-binding proteins. PLoS Genet. 3:e233.

Lee M-H, Ohmachi M, Arur S, Nayak S, Francis R, Church D, Lambie E, Schedl T. 2007b. Multiple functions and dynamic activation of MPK-1 extracellular signal-regulated kinase signaling in *Caenorhabditis elegans* germline development. Genetics. 177:2039–2062.

Lemmens BBLG, Tijsterman M. 2011. DNA double-strand break repair in *Caenorhabditis elegans*. Chromosoma. 120:1–21.

Lev I, Rechavi O. 2020. Germ granules allow transmission of small RNA-based parental responses in the "germ plasm." iScience. 23:101831.

Li Z, Luo L, Yu W, Li P, Ou D, Liu J, Ma H, Sun Q, Liang A, Huang C, *et al.* 2022. PPARγ phase separates with RXRα at PPREs to regulate target gene expression. Cell Discov. 8:37.

Lionaki E, Tavernarakis N. 2013. Assessing aging and senescent decline in *Caenorhabditis elegans*: cohort survival analysis. In: Galluzzi L, Vitale I, Kepp O, Kroemer G, editors. Methods in molecular biology. Totowa (NJ): Humana Press. p. 473–484.

Liu Y, Zhao Q, Nie H, Zhang F, Fu T, Zhang Z, Qi F, Wang R, Zhou J, Gao J. 2021. SYP-5 regulates meiotic thermotolerance in *Caenorhabditis elegans*. Yao X, editor. J Mol Cell Biol. 13:662–675.

Lopez AL III, Chen J, Joo H-J, Drake M, Shidate M, Kseib C, Arur S. 2013. DAF-2 and ERK couple nutrient availability to meiotic progression during *Caenorhabditis elegans* oogenesis. Dev Cell. 27:227–240.

Love MI, Huber W, Anders S. 2014. Moderated estimation of fold change and dispersion for RNA-seq data with DESeq2. Genome Biol. 15:550. https://doi.org/10.1186/s13059-014-0550-8.

Lu T, Mortimer M, Li F, Li Z, Chen L, Li M, Guo L-H. 2023. Putative adverse outcome pathways of the male reproductive toxicity derived from toxicological studies of perfluoroalkyl acids. Sci Total Environ. 873:162439.

Lui DY, Colaiácovo MP. 2013. Meiotic development in *Caenorhabditis elegans*. In: T Schedl, editor. Germ cell development in C. elegans. Vol. 757. New York (NY): Springer New York. p. 133–170.

Mainpal R, Priti A, Subramaniam K. 2011. PUF-8 suppresses the somatic transcription factor PAL-1 expression in *C. elegans* germline stem cells. Dev Biol. 360:195–207.

Manage KI, Rogers AK, Wallis DC, Uebel CJ, Anderson DC, Nguyen DAH, Arca K, Brown KC, Cordeiro Rodrigues RJ, de Albuquerque BFM, *et al.* 2020. A tudor domain protein, SIMR-1, promotes siRNA production at piRNA-targeted mRNAs in *C. elegans*. Elife. 9: e56731. https://doi.org/10.7554/elife.56731.

McEwen TJ, Yao Q, Yun S, Lee C-Y, Bennett KL. 2016. Small RNA in situ hybridization in *Caenorhabditis elegans*, combined with RNA-seq, identifies germline-enriched microRNAs. Dev Biol. 418:248–257.

Messina PV, Prieto G, Salgado F, Varela C, Nogueira M, Dodero V, Ruso JM, Sarmiento F. 2007. The influence of sodium perfluorooctanoate on the conformational transitions of human immunoglobulin. J Phys Chem B. 111:8045–8052.

Miller MA, Nguyen VQ, Lee MH, Kosinski M, Schedl T, Caprioli RM, Greenstein D. 2001. A sperm cytoskeletal protein that signals oocyte meiotic maturation and ovulation. Science. 291:2144–2147.

Minogue AL, Tackett MR, Atabakhsh E, Tejada G, Arur S. 2018. Functional genomic analysis identifies miRNA repertoire regulating *C. elegans* oocyte development. Nat Commun. 9:5318. https://doi.org/10.1038/s41467-018-07791-w.

Nadarajan S, Mohideen F, Tzur YB, Ferrandiz N, Crawley O, Montoya A, Faull P, Snijders AP, Cutillas PR, Jambhekar A, *et al.* 2016. The MAP kinase pathway coordinates crossover designation with disassembly of synaptonemal complex proteins during meiosis. Elife. 5:e12039. https://doi.org/10.7554/elife.12039.

Nakayama SF, Yoshikane M, Onoda Y, Nishihama Y, Iwai-Shimada M, Takagi M, Kobayashi Y, Isobe T. 2019. Worldwide trends in tracing poly- and perfluoroalkyl substances (PFAS) in the environment. Trends Analyt Chem. 121:115410.

Nass R, Hamza I. 2007. The nematode *C. elegans* as an animal model to explore toxicology in vivo: solid and axenic growth culture conditions and compound exposure parameters. Curr Protoc Toxicol. Chapter 1:Unit1.9. https://doi.org/10.1002/0471140856.tx0109s31.

Neves ARR, Čavka I, Rausch T, Köhler S. 2025. Crossovers are regulated by a conserved and disordered synaptonemal complex domain. Nucleic Acids Res. 53:gkaf095.

Pan Y, Zhang H, Cui Q, Sheng N, Yeung LWY, Sun Y, Guo Y, Dai J. 2018. Worldwide distribution of novel perfluoroether carboxylic and sulfonic acids in surface water. Environ Sci Technol. 52:7621–7629.

Parodi DA, Sjarif J, Chen Y, Allard P. 2015. Reproductive toxicity and meiotic dysfunction following exposure to the pesticides Maneb, Diazinon and Fenarimol. Toxicol Res. 4:645–654.

Patro R, Duggal G, Love MI, Irizarry RA, Kingsford C. 2017. Salmon provides fast and bias-aware quantification of transcript expression. Nat Methods. 14:417–419.

Pelch KE, Reade A, Kwiatkowski CF, Merced-Nieves FM, Cavalier H, Schultz K, Wolffe T, Varshavsky J. 2022. The PFAS-Tox database: a systematic evidence map of health studies on 29 per- and polyfluoroalkyl substances. Environ Int. 167:107408.

Prieto G, Sabín J, Ruso JM, González-Pérez A, Sarmiento F. 2004. A study of the interaction between proteins and fully-fluorinated and fully-hydrogenated surfactants by ζ-potential measurements. Colloids Surf A Physicochem Eng Asp. 249:51–55.

Rechavi O, Lev I. 2017. Principles of transgenerational small RNA inheritance in *Caenorhabditis elegans*. Curr Biol. 27:R720–R730. https://doi.org/10.1016/j.cub.2017.05.043.

Ripley BD. 2001. The R project in statistical computing. MSOR Connect. 1:23–25.

Rog O, Köhler S, Dernburg AF. 2017. The synaptonemal complex has liquid crystalline properties and spatially regulates meiotic recombination factors. Elife. 6:e21455.

Salwiczek M, Nyakatura EK, Gerling UIM, Ye S, Koksch B. 2012. Fluorinated amino acids: compatibility with native protein structures and effects on protein–protein interactions. Chem Soc Rev. 41:2135–2171.

Sanchez Garcia D, Sjödin M, Hellstrandh M, Norinder U, Nikiforova V, Lindberg J, Wincent E, Bergman Å, Cotgreave I, Munic Kos V. 2018. Cellular accumulation and lipid binding of perfluorinated alkylated substances (PFASs)—a comparison with lysosomotropic drugs. Chem Biol Interact. 281:1–10.

Sanchez-Burgos I, Joseph JA, Collepardo-Guevara R, Espinosa JR. 2021. Size conservation emerges spontaneously in biomolecular condensates formed by scaffolds and surfactant clients. Sci Rep. 11:15241.

Sapetschnig A, Sarkies P, Lehrbach NJ, Miska EA. 2015. Tertiary siRNAs mediate paramutation in *C. elegans*. PLoS Genet. 11: e1005078.

Scheckel C, Gaidatzis D, Wright JE, Ciosk R. 2012. Genome-wide analysis of GLD-1-mediated mRNA regulation suggests a role in mRNA storage. PLoS Genet. 8:e1002742.

Sendoel A, Subasic D, Ducoli L, Keller M, Michel E, Kohler I, Singh KD, Zheng X, Brümmer A, Imig J, *et al.* 2019. MINA-1 and WAGO-4 are part of regulatory network coordinating germ cell death and RNAi in *C. elegans*. Cell Death Differ. 26:2157–2178.

Seroussi U, Lugowski A, Wadi L, Lao RX, Willis AR, Zhao W, Sundby AE, Charlesworth AG, Reinke AW, Claycomb JM. 2023. A comprehensive survey of *C. elegans* argonaute proteins reveals organism-wide gene regulatory networks and functions. Elife. 12:e83853. https://doi.org/10.7554/elife.83853.

Shi Y, Vestergren R, Xu L, Zhou Z, Li C, Liang Y, Cai Y. 2016. Human exposure and elimination kinetics of chlorinated polyfluoroalkyl ether sulfonic acids (Cl-PFESAs). Environ Sci Technol. 50:2396–2404.

Smolikov S, Eizinger A, Schild-Prufert K, Hurlburt A, McDonald K, Engebrecht J, Villeneuve AM, Colaiácovo MP. 2007. SYP-3 restricts synaptonemal complex assembly to bridge paired chromosome axes during meiosis in *Caenorhabditis elegans*. Genetics. 176:2015–2025.

Srivastava A, Malik L, Smith T, Sudbery I, Patro R. 2019. Alevin efficiently estimates accurate gene abundances from dscRNA-seq data. Genome Biol. 20:65. https://doi.org/10.1186/s13059-019-1670-y.

Starich TA, Bai X, Greenstein D. 2020. Gap junctions deliver malonyl-CoA from soma to germline to support embryogenesis in *Caenorhabditis elegans*. eLife. 9:e58619.

Stylianou M, Bjornsdotter MK, Olsson PE, Ericson Jogsten I, Jass J. 2019. Distinct transcriptional response of *Caenorhabditis elegans* to different exposure routes of perfluorooctane sulfonic acid. Environ Res. 168:406–413.

Sundby AE, Molnar RI, Claycomb JM. 2021. Connecting the dots: linking *Caenorhabditis elegans* small RNA pathways and germ granules. Trends Cell Biol. 31:387–401.

Tabara H, Mitani S, Mochizuki M, Kohara Y, Nagata K. 2023. A small RNA system ensures accurate homologous pairing and unpaired silencing of meiotic chromosomes. Embo J. 42:e105002. https://doi.org/10.15252/embj.2020105002.

Tang H, Han M. 2017. Fatty acids regulate germline sex determination through ACS-4-dependent myristoylation. Cell. 169:457–469.e13.

Tran AT, Chapman EM, Flamand MN, Yu B, Krempel SJ, Duchaine TF, Eroglu M, Derry WB. 2019. MiR-35 buffers apoptosis thresholds in the *C. elegans* germline by antagonizing both MAPK and core apoptosis pathways. Cell Death Differ. 26:2637–2651.

Truong L, Chen Y-W, Barrere-Cain R, Levenson MT, Shuck K, Xiao W, da Veiga Beltrame E, Panter B, Reich E, Sternberg PW, *et al.* 2023. Single-nucleus resolution mapping of the adult *C. elegans* and its application to elucidate inter- and trans-generational response to alcohol. Cell Rep. 42:112535.

Ulaganathan G, Jiang H, Canio N, Oke A, Armstrong SS, Abrahamsson D, Varshavsky JR, Lam J, Cooper C, Robinson JF, *et al.* 2024. Screening and characterization of 133 physiologically-relevant environmental chemicals for reproductive toxicity. Reprod Toxicol. 126:108602.

United Nations Environment Program. 2023. Stockholm Convention on Persistent Organic Pollutants (POPs) Text and Annexes [accessed 2023 Aug 16]. https://www.pops.int/Portals/0/download.aspx?d=UNEP-POPS-COP-CONVTEXT-2023.English.pdf.

Updike DL, Hachey SJ, Kreher J, Strome S. 2011. P granules extend the nuclear pore complex environment in the *C. elegans* germ line. J Cell Biol. 192:939–948.

US Environmental Protection Agency. 2000. EPA and 3M announce phase out of PFOS [accessed 2025 Apr 24]. https://www.epa.gov/archive/epapages/newsroom_archive/newsreleases/33aa946e6cb11f35852568e1005246b4.html.

Vabre P, Gatimel N, Moreau J, Gayrard V, Picard-Hagen N, Parinaud J, Leandri RD. 2017. Environmental pollutants, a possible etiology for premature ovarian insufficiency: a narrative review of animal and human data. Environ Health. 16:37.

Vaid S, Ariz M, Chaturbedi A, Kumar GA, Subramaniam K. 2013. PUF-8 negatively regulates RAS/MAPK signalling to promote differentiation of *C. elegans* germ cells. Development. 140:1645–1654.

Wang M, Chen Y, Kickhoefer VA, Rome LH, Allard P, Mahendra S. 2019. A vault-encapsulated enzyme approach for efficient degradation and detoxification of bisphenol A and its analogues. ACS Sustain Chem Eng. 7:5808–5817.

Wang Y, Zhang H, Kang Y, Cao J. 2016. Effects of perfluorooctane sulfonate on the conformation and activity of bovine serum albumin. J Photochem Photobiol B. 159:66–73.

Wei K-N, Wang X-J, Zeng Z-C, Gu R-T, Deng S-Z, Jiang J, Xu C-L, Li W, Wang H-L. 2021. Perfluorooctane sulfonate affects mouse oocyte maturation in vitro by promoting oxidative stress and apoptosis induced by mitochondrial dysfunction. Ecotoxicol Environ Saf. 225:112807.

Xiong H, Pears C, Woollard A. 2017. An enhanced *C. elegans* based platform for toxicity assessment. Sci Rep. 7:9839. https://doi.org/10.1038/s41598-017-10454-3.

Xu Z, Zhao J, Hong M, Zeng C, Guang S, Shi Y. 2021. Structural recognition of the mRNA 3′ UTR by PUF-8 restricts the lifespan of *C. elegans*. Nucleic Acids Res. 49:10082–10097.

Yang W, Dierking K, Schulenburg H. 2016. WormExp: a web-based application for a *Caenorhabditis elegans*-specific gene expression enrichment analysis. Bioinformatics. 32:943–945.

Yin J, Jian Z, Zhu G, Yu X, Pu Y, Yin L, Wang D, Bu Y, Liu R. 2021. Male reproductive toxicity involved in spermatogenesis induced by perfluorooctane sulfonate and perfluorooctanoic acid in *Caenorhabditis elegans*. Environ Sci Pollut Res Int. 28:1443–1453.

Zhang Z, Xie S, Wang R, Guo S, Zhao Q, Nie H, Liu Y, Zhang F, Chen M, Liu L, *et al.* 2020. Multivalent weak interactions between assembly units drive synaptonemal complex formation. J Cell Biol. 219:e201910086.

Toxicological Sciences, 2025, 00, 1–21
https://doi.org/10.1093/toxsci/kfaf111
Research article